BRNO UNIVERSITY OF TECHNOLOGY

Faculty of Electrical Engineering
and Communication

MASTER'S THESIS

Brno, 2024 Bc. Matej Ledvina

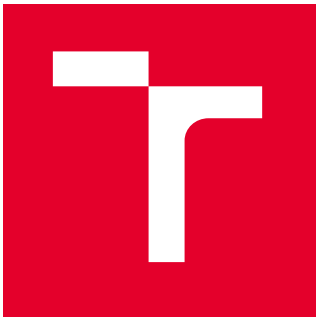

BRNO UNIVERSITY OF TECHNOLOGY

VYSOKÉ UČENÍ TECHNICKÉ V BRNĚ

FACULTY OF ELECTRICAL ENGINEERING AND COMMUNICATION

FAKULTA ELEKTROTECHNIKY
A KOMUNIKAČNÍCH TECHNOLOGIÍ

DEPARTMENT OF RADIO ELECTRONICS

ÚSTAV RADIOELEKTRONIKY

STUDY OF CHAOTIC OSCILLATORS HAVING PASSIVE FRACTAL TWO-TERMINAL ELEMENTS

STUDIUM CHAOTICKÝCH OSCILÁTORŮ S PASIVNÍMI FRAKTÁLNÍMI DVOJPÓLY

MASTER'S THESIS
DIPLOMOVÁ PRÁCE

AUTHOR
AUTOR PRÁCE

Bc. Matej Ledvina

SUPERVISOR
VEDOUCÍ PRÁCE

doc. Ing. Jiří Petržela, Ph.D.

BRNO 2024

BRNO UNIVERSITY OF TECHNOLOGY
FACULTY OF ELECTRICAL ENGINEERING AND COMMUNICATION

Master's Thesis

Master's study program **Electronics and Communication Technologies**

Department of Radio Electronics

Student: Bc. Matej Ledvina ***ID:*** 221339

Year of study: 2 ***Academic year:*** 2023/24

TITLE OF THESIS:

Study of chaotic oscillators having passive fractal two-terminal elements

INSTRUCTION:

Become familiar with problems involving circuit synthesis of chaotic systems based on known set of ordinary differential equations. Study well-established methods of design of passive two-terminal elements which approximate fractional-order capacitor in predefined frequency range. Design and verify few such two-terminal elements, both using computer-aided analysis and experimental measurement. Choose suitable mathematical model of autonomous chaotic system and practically implement it as lumped electronic circuit. Its correct function should be verified by means of Orcad Pspice circuit simulator.

Designed chaotic oscillator should be practically realized and verified via detailed measurement. Try to capture interesting dynamical behavior for non-nteger orders of differential equations, i.e., conventional capacitors should be replaced by fractional counterparts. Finally, compare achieved results with numerical analysis, discuss differencies between theory and practical measurement.

RECOMMENDED LITERATURE:

[1] PETRŽELA, Jiří. Accurate constant phase elements dedicated for audio signal processing. Applied Sciences - Basel, 2019, roč. 9, č. 22, s. 1-35. ISSN: 2076-3417.

[2] RUJZL, Miroslav, POLÁK, Ladislav a Jiří PETRŽELA. Hybrid Analog Computer for Modeling Nonlinear Dynamical Systems: The Complete Cookbook. SENSORS, 2023, roč. 23, č. 7, s. 1-17. ISSN: 1424-8220.

Date of project specification: 16.2.2024 ***Deadline for submission:*** 20.5.2024

Supervisor: doc. Ing. Jiří Petržela, Ph.D.

doc. Ing. Lucie Hudcová, Ph.D.
Chair of study program board

ABSTRACT

This thesis deals with chaotic circuits of fractional order. First, an overview of fractal elements and their approximations is presented. Three fractal element approximations are then realized and tested. Next, a short overview of chaotic systems is presented and methods of synthesizing such systems into electrical circuits is discussed. Two methods are selected, and an example of synthesis with both methods is performed. Next, a known system with observed chaotic behavior is synthesized into a circuit, simulated, built. and experimentally verified.

KEYWORDS

Fractal elements, fractal element approximations, Chua circuit, chaos, fractional order chaotic systems

ABSTRAKT

Táto semestrálna práca sa zaoberá chaotickými obvodmi s fraktálnymi prvkami. V prvej časti sú prezentované fraktálne prvky, ich vlastnosti a spôsob syntézy. Tri takéto prvky sú navrhnuté, vyhotovené a merané. V druhej časti je krátky úvod do problematiky chaotických obvodov, a spôsobov ich syntézy. Následne sú prezentované dve metódy syntézy chaotických obvodov s názorným príkladom. Na koniec bol vybraný jeden chaotický system ktorý bol syntetizovaný do obvodu, odsimulovaný, zhotovený a experimentálne overený.

KĽÚČOVÉ SLOVÁ

Fraktálne prvky, aproximácie fraktálnych prvkov, Chuov obvod, chaos, chaotické systémy fraktálneho rádu.

Bibliographic citation

LEDVINA, Matej. *Studium chaotických oscilátorů s pasivními fraktálními dvojpóly.* Brno, 2024. Dostupné také z: https://www.vut.cz/studenti/zav-prace/detail/159066. Diplomová práce. Vysoké učení technické v Brně, Fakulta elektrotechniky a komunikačních technologií, Ústav radioelektroniky. Vedoucí práce Jiří Petržela.

Author's Declaration

I declare that I have written this paper independently, under the guidance of the advisor and using exclusively the technical references and other sources of information cited in the project and listed in the comprehensive bibliography at the end of the project.

As the author, I furthermore declare that, with respect to the creation of this paper, I have not infringed any copyright or violated anyone's personal and/or ownership rights. In this context, I am fully aware of the consequences of breaking Regulation S 11 of the Copyright Act No. 121/2000 Coll. of the Czech Republic, as amended, and of any breach of rights related to intellectual property or introduced within amendments to relevant Acts such as the Intellectual Property Act or the Criminal Code, Act No. 40/2009 Coll., Section 2, Head VI, Part 4.

.

Brno, _____ _____

author's signature

CONTENTS

FIGURES

TABLES

INTRODUCTION

Chaos in electrical circuits has been a point of interest for researchers and engineers for some time now. Chaotic behavior is special because while deterministic, it is very unpredictable. With its many useful properties and promising real-world applications, a sizable amount of research is being conducted on studying chaos in electronics.

Another promising field are fractal elements. They are circuit elements that inhibit the properties of partially a capacitor, or inductor, and partially that, of a resistor. These elements allow researchers to create more precise models of the real world. This thesis aims to study some of the properties of fractal chaotic systems.

The first chapter aims to introduce fractal elements and the way they can be created. Next, three different fractal elements are designed, built, and simulated and their behavior is measured and compared to the mathematical models. The third chapter provides an introduction to chaotic systems and discusses the fractal ones. Next, two methods of synthesis of chaotic circuits are chosen and each method is demonstrated on a simple example. In the fifth chapter of the thesis, a system is selected which is then synthesized into an electrical circuit. This circuit is then simulated in SPICE program and results are discussed. The last chapter of the thesis discusses real realization of the circuit, which is built, measured and the result are presented. At last, a complete model of the circuit is created and a numerical analysis is performed.

1. INTRODUCTION TO FRACTAL ELEMENTS

Fractional calculus, a more expanded form of traditional calculus has relatively recently found it's practical applications in linear systems and signals [1]. Introducing fractional derivatives into linear circuit theory allows for description of a new type of component, commonly referred to as a constant phase element (CPE) [3]. As of now, the CPE is unfortunately not commercially available as an electrical component, despite previous efforts [4]. The behavior of an ideal CPE can however be approximated in a limited frequency range. The CPE that will be utilized in this thesis - a fractal capacitor, will be an approximation of an ideal one using common passive components.

1.1 Ideal CPE

Behavior of an ideal CPE in frequency domain can be described by a generalized formulas of passive two-terminal elements from linear circuit theory [5]. The 3 basic passive elements: resistor, capacitor and an inductor are depicted below, complemented with their corresponding impedance functions obtained from the Laplace transform. The 4th depicted element is a frequency dependent negative resistor (FDNR), which as a real component is only available in synthetic form [6].

$Z_R(s) = R$ $Z_C(s) = \frac{1}{sC}$ $Z_L(s) = sL$ $Z_D(s) = \frac{1}{Ds^2}$

a) b) c) d)

Figure 1.1 – Symbol and impedance function for a) resistor, b) capacitor, c) inductor, d) FDNR

Modifying the impedance function of a capacitor and inductor in the following manner will allow us to describe all of the basic passive elements as well as the CPE:

$$Y_C(s) = Y_\beta \cdot s^\alpha \qquad Z_L(s) = Z_\alpha \cdot s^\beta \tag{1.1}$$

In case when α and β are 1, these equations yield the original functions for C and L respectively. In case when either α or β is 2, the resulting function describes a FDNR, and a 0 will yield the resistor impedance function. For $\beta \in (0, 1)$ the function

describes a fractal inductor, while $\alpha \in (0, 1)$ describes a fractal capacitor [7]. A CPE is therefore a component partially exhibiting characteristics of a resistor, and partially of a capacitor or an inductor. Figure 1.2 shows the placement of all linear passive elements as well as the fractal inductor and capacitor in the frequency domain.

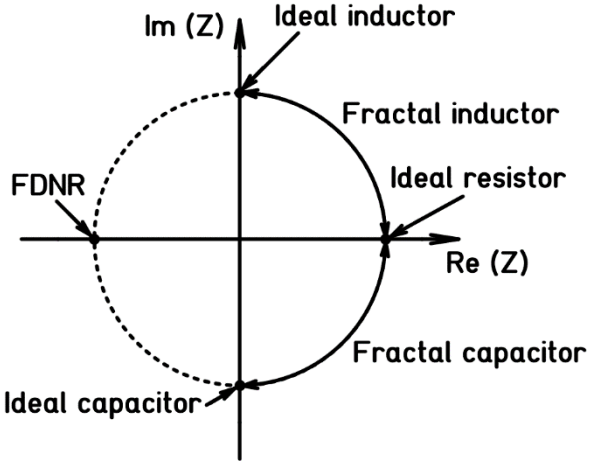

Figure 1.2 Complex plane with locations of all linear passive elements as well as the fractal inductor and capacitor

A fractal element is characterized by two parameters, it's phase shift and impedance. The impedance of a CPE is usually referred to as fractance (designated D), expressed as $\left[\mathrm{H} \cdot \mathrm{s}^{1-\beta}\right]$ in case of fractional inductance, and $[\mathrm{F}/\mathrm{s}^{1-\alpha}]$ in case of fractional capacitance [8]. Extracting the frequency and phase response for the fractal capacitor shows that its impedance decreases with frequency at a slope of $\alpha \cdot 20$ dB per decade and its phase shift is constant, precisely $\alpha \cdot -90$ degrees. For the fractal inductor the relations are, as expected inverted.

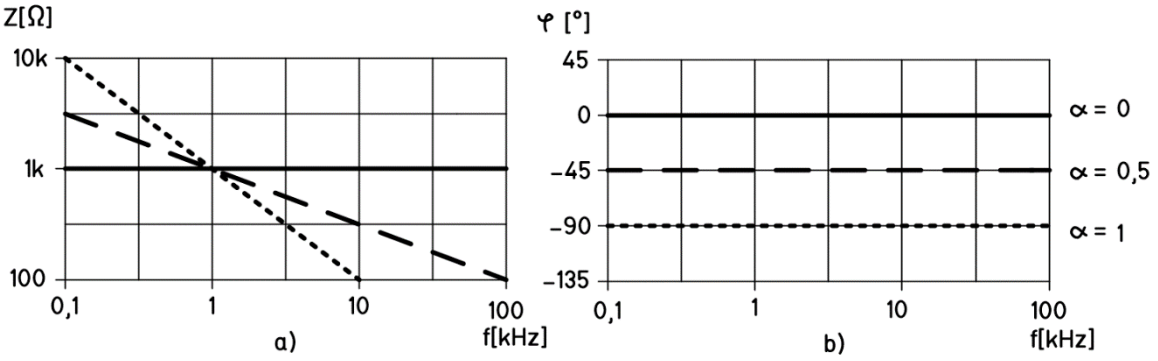

Figure 1.3 a) Impedance and b) Phase response for resistor (α = 0), fractal capacitor (α = 0,5) and ideal capacitor (α = 1)

1.2 CPE Approximation

A viable method of approximating a CPE is with a network model. Forming a network consisting of basic passive components can yield a two-terminal device that can in a limited frequency range approximate the behavior of a fractal element. Several methods for this type of approximation were proposed in the past, many however depend on various numeric iteration methods or optimization algorithms [9]. Some methods depend on active elements or negative resistances or form two-port instead of two-terminal devices, which limit's their application [10][11]. A very straight-forward method for constructing the network is described in [12] which will be the one utilized in this thesis.

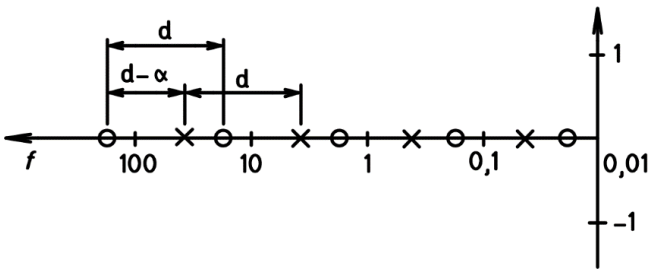

Figure 1.4 Example of an equidistant zero-pole distribution

This method generates a network with an equidistant distribution (in logarithmic measure) of repeating zeroes and poles in left half plane, depicted on Figure 1.4. With a finite number of these zeroes and poles it is possible to approximate a CPE in a limited frequency range with a steady phase angle of any value a minimum phase system can have (-90° to 90°) [13]. The phase response will however never be completely straight, a quantifiable ripple will be always present, dependent on the distance *d*. The impedance function for such network can be written as follows

$$Y_C(s) = Y_0 \frac{\prod_{i=1}^{m}(s - z_i)}{\prod_{i=1}^{n}(s - p_i)} \qquad Z_L(s) = Z_0 \frac{\prod_{i=1}^{m}(s - z_i)}{\prod_{i=1}^{n}(s - p_i)} \tag{1.2}$$

where *m = n*. The schematic diagram on Figure 1.5, depicts two circuit realizations

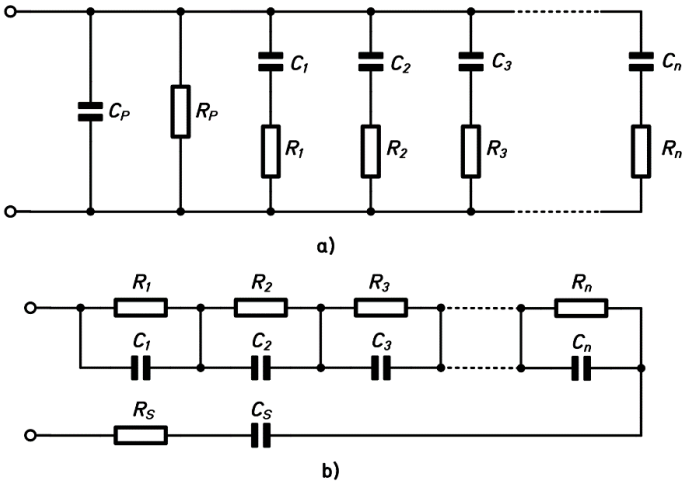

Figure 1.5 Schematic diagram of two CPE networks

containing only resistors and capacitors. Such CPE will have characteristics of a fractal capacitor, however, a fractal inductor can be created in very much the same way using the duality principle. Input impedance for configuration on Figure 1.5a can be expressed as

$$Y_C(s) = \frac{1}{R_P} + sC_P + \sum_{i=1}^{n} \frac{sC_i}{sC_iR_i + 1}. \tag{1.3}$$

Each of the R-C pairs generates one of the pole-zero pairs in the polar plot, while the C_P and R_P are referred to in the paper as correction elements. They define the corner frequencies and help to extend the usable frequency range of the approximation. The following can be written about the amplitude and phase response of the Figure 1.5a network:

$$\lim_{\omega\to 0} \arg Z_C(\, s = j\omega) = 0, \qquad \lim_{\omega\to \infty} \arg Z_C(s = j\omega) = -\frac{\pi}{2}, \tag{1.4}$$

$$\lim_{\omega\to 0} |Z_C(s = j\omega)| = R_P, \qquad \lim_{\omega\to \infty} |Z_C(s = j\omega)| = 0\,. \tag{1.5}$$

Similarly, the Figure 1.5b network can be described

$$Z_C(s) = R_s + \frac{1}{sC_s} + \sum_{i=1}^{n} \frac{R_i}{sC_i + 1}, \tag{1.6}$$

$$\lim_{\omega\to 0} \arg Z_C(s = j\omega) = -\frac{\pi}{2}, \qquad \lim_{\omega\to \infty} \arg Z_C(s = j\omega) = 0, \tag{1.7}$$

$$\lim_{\omega\to 0} |Z_C(s = j\omega)| = \infty, \qquad \lim_{\omega\to \infty} |Z_C(s = j\omega)| = R_S\,. \tag{1.8}$$

2. BUILDING THE FRACTAL CAPACITORS

The CPE approximations were designed using network models created by an algorithm described in [14]. We start by selecting design parameters of the CPE model. These are the corner frequencies f_{min} and f_{max} calculated from the time constant $\tau_1 = R_1C_1$, phase ripple $\Delta\varphi$, desired phase angle φ, number of RC sections in the network, and the fractance D. From description of the design method in Chapter 1.2 it is clear that some input parameters lead to contradicting results. For example, the desired frequency range cannot be obtained if insufficient number of sections, too low phase angle or too small of a phase ripple is chosen.

The constructed fractal capacitors are to be used in a chaotic oscillator. These are wideband circuits, therefore a steady phase angle over a large frequency range is desired. The range of 10 Hz to 1 MHz was decided as sufficient for this application. Another important parameter is the phase ripple. It was decided that $\Delta\varphi < 1°$ is acceptable, however because we must use commercially available components, which have values dictated by the E series of preferred values and manufacturing tolerances the calculation will be performed for lower value of $\Delta\varphi$ to make up for these limitations. Under these conditions a number of sections sufficient for a good approximation is 9. More sections could lead to wider range or smaller ripple; however, it was discovered that more than 10 sections will end up hindering, rather than improving the model accuracy because manufacturing tolerances with such large number of devices become unmanageable. 3 fractal capacitors were designed, with α = ¼, ½ and ¾. The structure a) from Figure 1.5 was chosen as more fitting with the chosen parameters. The design variables are as summarized in Table 2.1.

α [-]	φ [°]	$\Delta\varphi$ [°]	n [-]	D [$F/s^{1-\alpha}$]
¼	22,5	0,1	9	13,11k
½	45	0,22	9	174,08k
¾	67,5	0,35	9	2,297M

Table 2.1 Input parameters of the 3 fractal capacitors.

The modulus of the ideal fractal capacitor at a given frequency can be derived from formula (1.1) (now denoting fractance with D instead of Y_C for clarity) this way:

$$|Z| = \frac{D}{(2\pi \cdot f)^{\alpha}} \ [\Omega] \tag{2.1}$$

The values for D in Table 2.1 are calculated such, that a 1 kΩ resistor, a 33 nF capacitor and all of the fractal capacitors will have the same modulus at frequency f = 4,823 kHz. This is also a design requirement for the chaotic system.

After all the component values are calculated, it is necessary to adjust them so that real components can be used for construction. This was accomplished by simulating all of the fractal capacitors in ORCAD PSpice and adjusting all the values one by one to fit into the desired $\Delta\varphi$ < 1°. In several instances it was necessary to cascade multiple components in parallel or series to achieve the desired phase ripple. Table 2.2 – Table 2.4 contain all the calculated and selected component values as well as the % error. The || notation is used for parallel combination of multiple components, while & is used for series combination. Component designated R_0 and C_0 are the parallel correction elements. Final component values are in rows marked with '.

n [-]	R_n [Ω]	R_n' [Ω]	ΔR [%]	C_n [F]	C_n' [F]	ΔC [%]
0	7,2631 k	7,5 k	3,16	96,777 p	82 p	18,0
1	15,681 k	15 k	4,54	1,9131 µ	1 µ || 1 µ	4,34
2	10,717 k	11 k	2,57	610,74 n	680 n	10,2
3	7,3247 k	7,15 k	1,73	194,97 n	220 n	11,4
4	5,0060 k	5 k	0,12	62,242 n	68 n	8,47
5	3,4214 k	3,3 k	3,68	19,870 n	18 n || 5,6 n	18,77
6	2,3383 k	2,2 k	6,29	6,342 n	6,8 n	6,74
7	1,5981 k	1,5 k	6,54	2,0250 n	2,2 n	7,95
8	1,0922 k	1 k	9,22	646,46 p	680 p	4,93
9	746,476	680	9,78	206,37 p	220 p	6,20

Table 2.2 Component values for the fractal capacitor network for α = ¼.

n [-]	R_n [Ω]	R_n' [Ω]	ΔR [%]	C_n [F]	C_n' [F]	ΔC [%]
0	84,076 k	82 k	2,53	534,39 p	560 p	4,57
1	67,013 k	68 k	8,09	447,67 n	1 µ & 1 µ	4,75
2	29,722 k	30 k	2,49	198,56 n	100 n || 100 n	0,72
3	13,183 k	13 k	1,41	88,067 n	82 n || 8,2 n	0,15
4	5,8470 k	6,2 k	5,69	39,061 n	68 n & 82 n	5,07
5	2,5934 k	2,7 k	4,12	17,325 n	18 n	3,75
6	1,1502 k	1,2 k	4,15	7,6841 n	8,2 n	6,29
7	510,167	510	0,03	3,4081 n	3,6 n	5,33
8	226,276	240	5,72	1,5116 n	1,6 n	5,55
9	100,361	100	0,36	670,45 p	680 p	1,40

Table 2.3 Component values for the fractal capacitor network for α = ½.

n [-]	R_n [Ω]	R_n' [Ω]	ΔR [%]	C_n [F]	C_n' [F]	ΔC [%]
0	1,1450 M	1,2 M	4,58	4,0672 n	3,9 n	4,29
1	431,67 k	470 k	8,16	69,497 n	68 n	2,20
2	118,19 k	120 k	1,51	45,127 n	12 n || 33 n	0,28
3	32,357 k	33 k	1,95	29,302 n	18 n || 12 n	1,74
4	8,8589 k	9,1 k	2,65	19,027 n	18 n	5,70
5	2,4254 k	2,7 k	10,2	12,355 n	12 n	2,96
6	664,043	680	2,35	8,0226 n	8,2 n	2,16
7	181,804	180	1,02	5,2093 n	5,1 n	2,14
8	49,7751	51	2,40	3,3826 n	3,3 n	2,50
9	13,6276	15	9,15	2,1964 n	2,2 n	0,16

Table 2.4 Component values for the fractal capacitor network for α = ¾.

Despite some values deviating by more than 10% it does not necessarily mean the approximation will be significantly off. If other elements around were also adjusted. This must be done experimentally because the overall phase response is dependent at any point on the values of most other components. Components chosen for the construction were of SMD type, size 0603. Resistors had 1% tolerance and capacitors had 5% tolerance. With the final component values a 100 run Monte Carlo analysis was performed to evaluate how manufacturing tolerances would impact the phase response. Figure 2.2 – Figure 2.3 show the results of the Monte Carlo analysis. It is obvious that the spread of the phase ripple is large. More than 4 degrees, which is not acceptable for this application. It is therefore necessary to hand-pick the components that will be used, by measuring multiple units and picking the one closest to the nominal value.

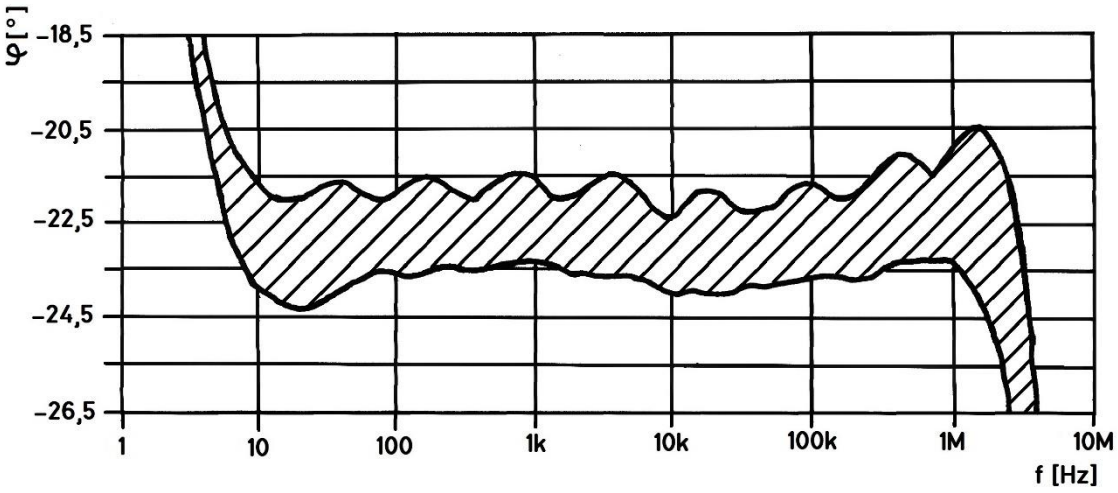

Figure 2.1 Spread of the phase response with 100 runs of Monte Carlo for the α = ¼ fractal capacitor

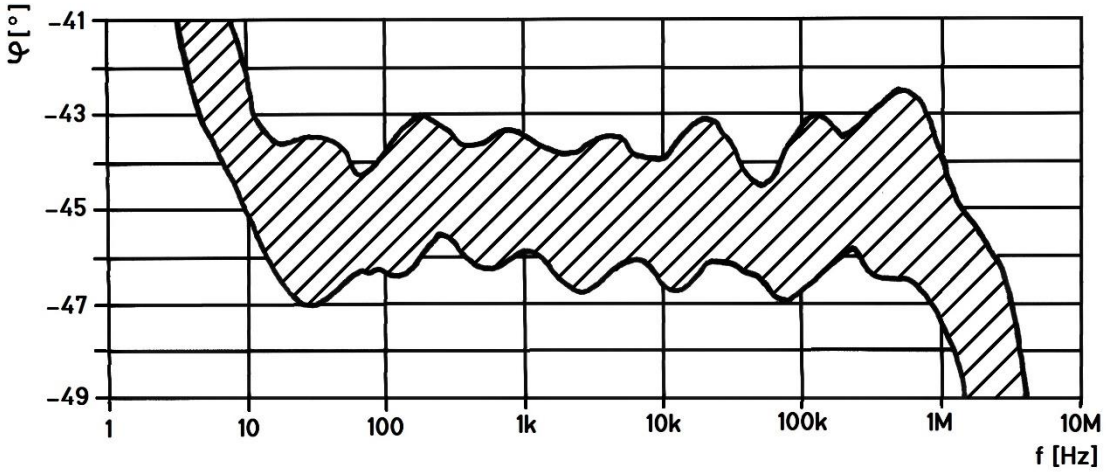

Figure 2.2 Spread of the phase response with 100 runs of Monte Carlo for the α = ½ fractal capacitor

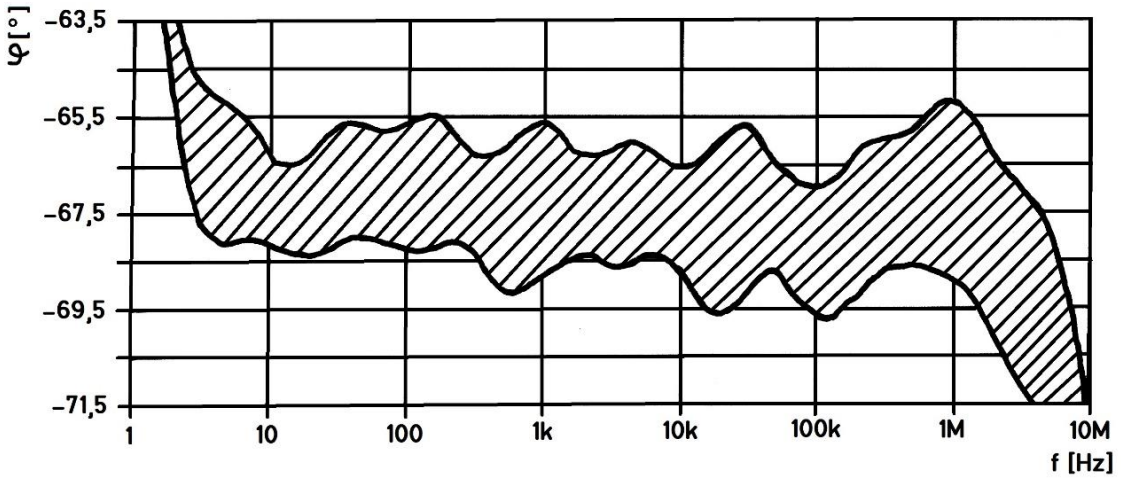

Figure 2.3 Spread of the phase response with 100 runs of Monte Carlo for the α = ¾ fractal capacitor

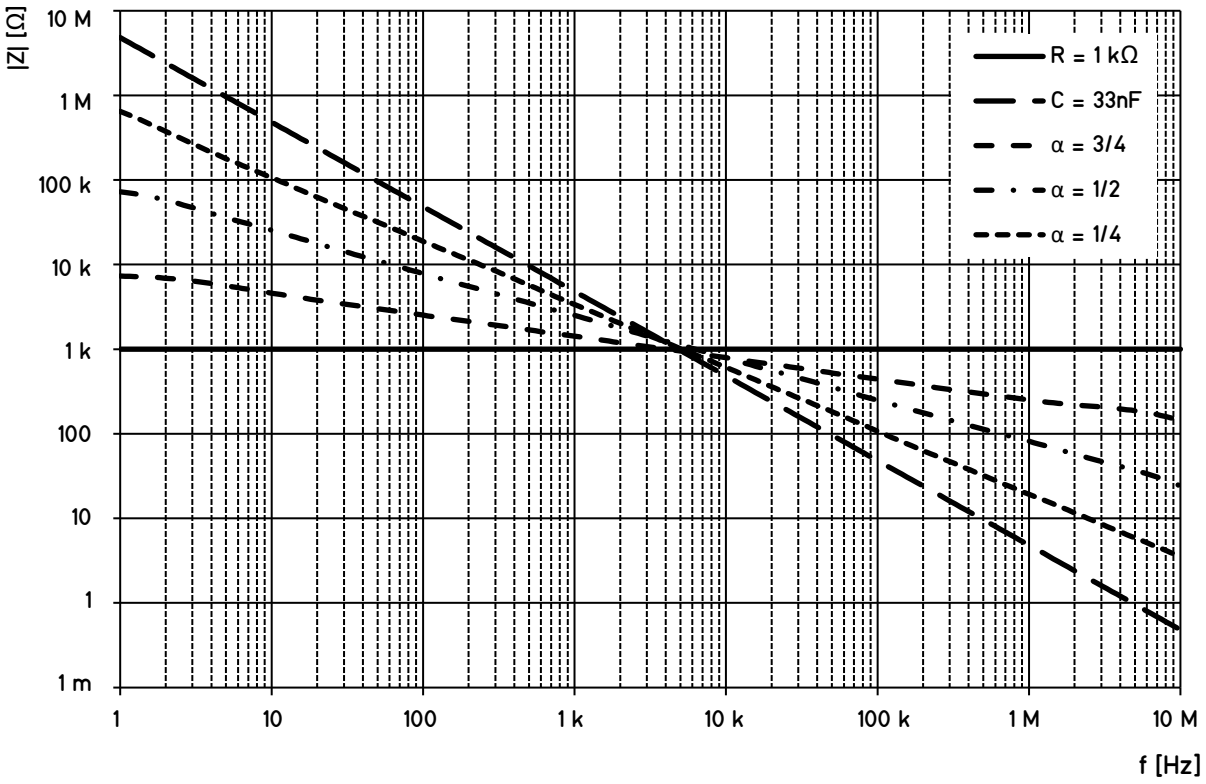

Figure 2.4 Modulus of impedance plotted for all fractal capacitors as well as a 33 nF capacitor and a 1 kΩ resistor

Figure 2.4 shows the impedance modulus of all of the simulated fractal elements, as well as a 1 kΩ resistor and a 33 nF capacitor. It is clear that all of the components have the same impedance at the same frequency and the slope of the fractal

elements is more moderate than that of a capacitor and corresponds to the α exponent.

The 3 fractal elements were constructed each on their own universal PCB. Next, AD844 [15] amplifier was set up in a fractional integrator configuration with the CPE and a single resistor setting the gain. The measurement was performer on the Keysight DSOX3022T digital oscilloscope, using the bode plot function. Figure 2.5 shows the phase relations for all 3 fractal elements.

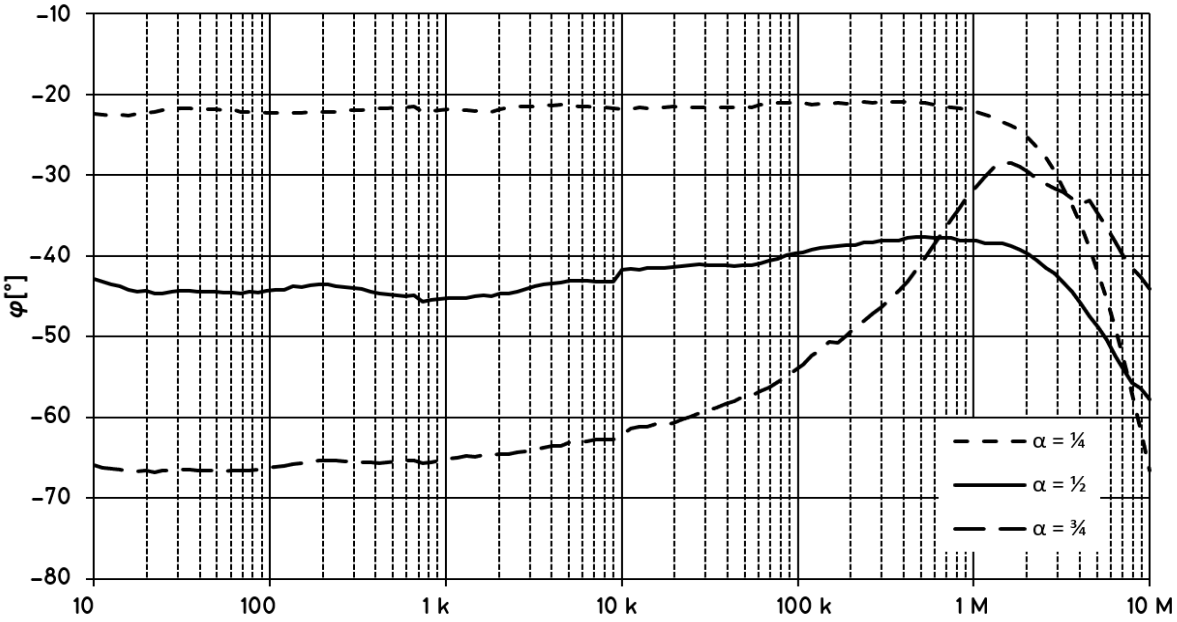

Figure 2.5 Measured phase angle response of all 3 constructed fractal capacitors

From the measured results several observations can be made. First, the AD844's limited bandwidth makes the measured data valid only up to 1 MHz. Second, the impedance norm of the CPE's with α = ½ and ¾ is too high, making measurements difficult. The parasitic capacitances in the measurement circuit create additional phase shift which is visible in the results. The approximation with α = ¼ is pretty accurate, with phase ripple corresponding to the simulated results, from this observation, and by looking at the results in the first two decades of the measurement for the other two CPE's, it could be assumed that the other two fractional capacitors also have phase responses similar to the simulated data. These fractal elements were therefore deemed suitable for use with the chaotic circuit.

3. CHAOTIC CIRUITS

Chaotic behavior, while lending itself similar to randomness is not at all related. While random behavior can be described by statistics and probability, chaos is unpredictable and deterministic, Chaotic circuits are of interest because of their potential in cryptography and communications [16][17]. The most known chaotic circuit to this day is the Chua's oscillator [18], discovered in 1983 and named after its creator L. O. Chua, which sparked a large interest in the search for more chaotic circuits, namely because of its simplicity. The circuit is a 3rd order system containing only 5 passive components and an active nonlinear component in form of a synthetic negative resistor, referred to as a Chua diode. Over the years countless modifications of this circuit have been a subject of scientific publications, adding more attractors, or using different nonlinearities [19]. This was however not the first chaotic system discovered. Credit for the first confirmed chaotic system goes to Edward Lorenz who discovered the system of 3 equations bearing his name in 1963.

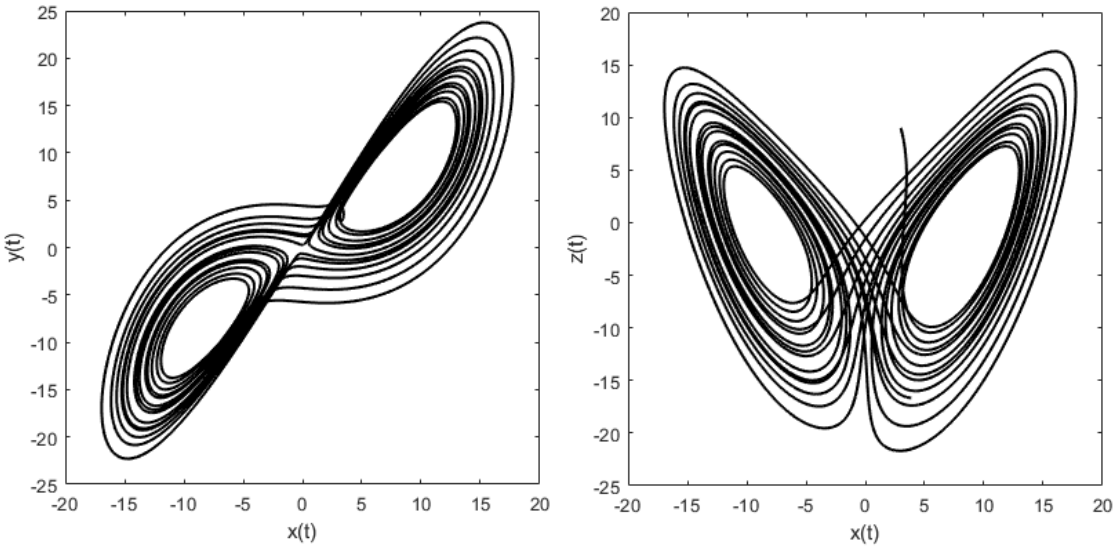

Figure 3.1 Double scroll attractor generated by the Lorenz system using numerical integration in MATLAB.

3.1 Description

What causes a system to behave in a chaotic manner is the presence of more than two state variables and presence of some nonlinearity [20]. Dynamic systems have

attractors, which determine their behavior in time. The trajectory of chaotic systems around the attractors is chaotic, highly sensitive on initial conditions and unpredictable. Attractors of chaotic systems can be very diverse and can take many visually enticing shapes. Signals created by chaotic circuits are often noise-like both in time and frequency domain, creating wide-band spectra rich with harmonic content [21]. Chaotic circuits must contain active elements and be at least of the 3rd order for autonomous circuits and of the 2nd for driven ones. Chaotic circuits come to existence in many ways. Accidental discovery of chaotic behavior is common. If the system meets the above-mentioned conditions, then under the right circumstances chaotic behavior can occur. Intentional design of chaotic circuits is possible by modifying existing circuits by adding non-linearities and additional degrees of freedom [22]. A more systematic approach can however be used to synthesize chaotic circuits. Starting with mathematical model; a set of differential equations which describe a known chaotic system a standard process of linear synthesis can be used to create a chaotic circuit [23]. This thesis will use the last of the mentioned approaches.

3.2 Fractional order chaotic circuits

Fractional order circuits can exhibit chaotic behavior same as integer order ones. One advantage of constructing with fractional elements is that the final circuit can be of less than 3rd order which is normally required for chaotic behavior to occur. It is however important to note that this is not the case for every single chaotic circuit. Fractional order chaotic circuits can be constructed either by synthesis from an already known set of fractional order differential equations [24] or by swapping capacitors or inductors in an already designed chaotic circuit for their fractional counterparts [25]. The latter method will be used in this thesis to construct the final chaotic oscillator. In this thesis an attempt will be made to experimentally prove a hypothesis, that swapping a fractal element with sufficiently small α in the place of its integer order counterpart, the chaotic behavior of the circuit will disappear and only harmonic oscillation will remain.

4. SYNTHESIS OF THE CHAOTIC CIRCUIT

The procedure of synthesizing chaotic circuits from a mathematical model is described in this chapter. Two approaches are presented, both of which are described in [26]. For simplicity the Chua's oscillator will be used as an example [27]. Suppose a known chaotic system described by a set of 3 differential equations

$$\begin{aligned} \frac{dx}{dt} &= \alpha(y - x - f(x)), \\ \frac{dy}{dt} &= x - y + z, \\ \frac{dz}{dt} &= -\beta(y + \gamma z). \end{aligned} \tag{4.1}$$

Where α, β and γ are dimensionless parameters and function $f(x)$ is a nonlinear function, in this case a PWL function described as

$$f(x) = \begin{cases} bx + a - b, & \text{for } x \geq 1, \\ ax, & \text{for } |x| < 1, \\ bx - a + b & \text{for } x \leq -1. \end{cases} \tag{4.2}$$

4.1 Classical circuit synthesis

First, we fold the system of 3 ordinary differential equations into a single third order function, by the process described in [28]. We express y from the third equation:

$$y = \frac{z' + \beta\gamma z}{-\beta}. \tag{4.3}$$

Then raise the order of the third equation and substitute for y which yields

$$z'' = -\beta(y' + \gamma z') = -\beta\left(x - \frac{z' + \beta\gamma z}{-\beta} + z\right) - \beta\gamma z'. \tag{4.4}$$

We then express x from (4.4) which yields

$$x = \frac{z'' + \beta(y' + \gamma z') + \beta\gamma z'}{-z' - \beta\gamma z} - z. \tag{4.5}$$

We then raise (4.4) again, to obtain

$$z''' = -\beta(y'' + \gamma z'') = -\beta(x - y + z) + \beta^2\gamma(y' + \gamma z'). \tag{4.6}$$

When we substitute x and y we get our third order function for system (4.2)

$$z''' + z''(\beta\gamma + a + 1) + z'(\beta + \beta\gamma + a\beta\gamma) + a\beta z$$
$$= a\beta f\left(-\frac{z'' + z''(\beta\gamma + 1) + z(\beta + \beta\gamma)}{\beta}\right). \tag{4.7}$$

Next we set

$$u(t) = \frac{z'' + z'(\beta\gamma + 1) + z(\beta + \beta\gamma)}{\beta},$$
$$i(t) = \frac{z''' + z''(\beta\gamma + a + 1) + z'(\beta + \beta\gamma + a\beta\gamma) + a\beta z}{a\beta} \tag{4.8}$$

and write the admittance function and apply the Laplace transform as follows:

$$Y(s) = \frac{\mathcal{L}\{i(t)\}}{\mathcal{L}\{u(t)\}}. \tag{4.9}$$

The obtained admittance function in s domain can now be written as

$$Y(s) = \frac{s^3 + s^2(\beta\gamma + a + 1) + s(\beta + \beta\gamma + a\beta\gamma) + a\beta}{a(s^2 + s(\beta\gamma + 1) + \beta + \beta\gamma)}. \tag{4.10}$$

We can now rewrite this function into a form that can be directly realized as an electrical circuit. In this example expansion into a continued fraction will yield

$$Y(s) = \frac{s}{a} + \cfrac{1}{1 + \cfrac{1}{s + \cfrac{1}{\cfrac{s}{\beta} + \gamma}}}, \tag{4.11a}$$

$$Y(s) = \frac{sC_1}{a} + \cfrac{1}{R_1 + \cfrac{1}{sC_2 + \cfrac{1}{\cfrac{sL}{\beta} + \gamma R_2}}}. \tag{4.11b}$$

In this form, the admittance function can be realized. There are more than one possible circuit realizations for a given admittance function, depending on what mathematical operations are performed during the synthesis. This creates an opportunity to pick the most practical one, be it by number of components, their

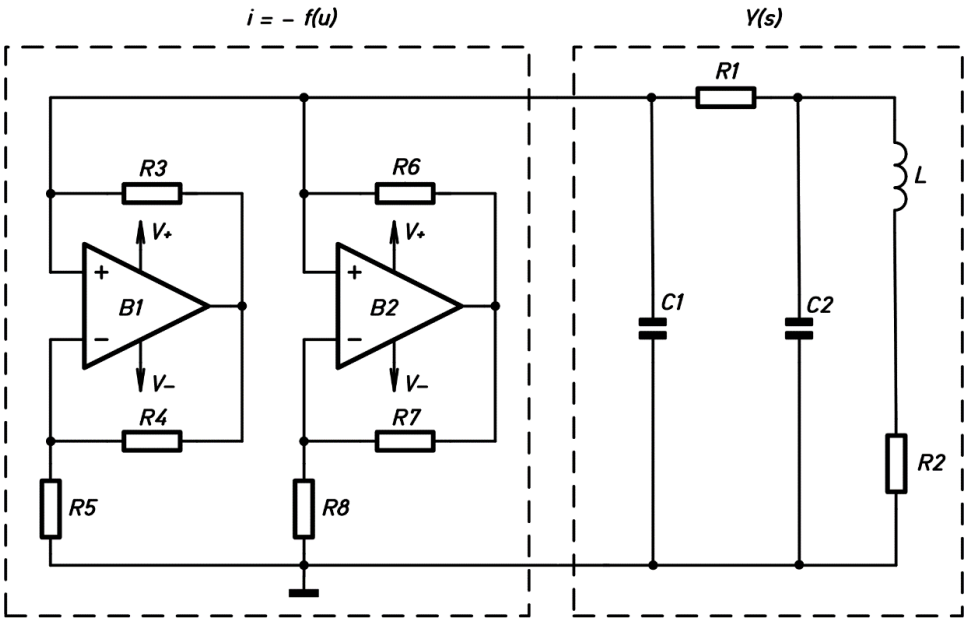

Figure 4.1 Schematic diagram of the Chua chaotic oscillator.

values or another design requirement. It might be possible that a solution does not exist at all, and a different method would have to be used such as separation into partial fractions, or other discussed in [23] . Negative component values cannot be realized in a passive circuit, so it may be necessary to use active components.

In the next step the non-linear function (4.2) is synthesized. Unfortunately, we cannot use linear circuit synthesis here and no other universal design process exists. If however a non-linear circuit realization with properties that fit the function description is known, we can directly connect it to the linear part of the system. To realize (4.2) we can for example use two synthetic negative resistors connected in parallel. The final chaotic circuit is depicted on Figure 4.1. Mathematical description of the non-linear part, assuming rail to rail operational amplifiers is as follows:

$$f(u) = \begin{cases} \dfrac{u}{R_3 || R_6}, & \text{for} \quad u \geq \dfrac{U_+}{A_1}, \\ \dfrac{u}{-R_5 || R_6}, & \text{for} \quad \dfrac{U_+}{A_1} > u \geq \dfrac{U_+}{A_2}, \\ \dfrac{u}{-R_5 || -R_8}, & \text{for} \quad \dfrac{U_+}{A_2} > u > \dfrac{U_-}{A_2}, \\ \dfrac{u}{-R_5 || R_6}, & \text{for} \quad \dfrac{U_-}{A_2} \geq u > \dfrac{U_-}{A_1}, \\ \dfrac{u}{R_3 || R_6}, & \text{for} \quad u \leq \dfrac{U_-}{A_1}, \end{cases} \tag{4.12}$$

where

$$R_3 = R_4,\ R_6 = R_7,\ A_1 = 1 + \frac{R_4}{R_5},\ A_2 = 1 + \frac{R_7}{R_8},\ A_1 < A_2. \tag{4.13}$$

For $U_+ / A_1 < u < U_- / A_1$ with a correct selection of gain for both amplifiers this circuit behaves like the nonlinear function described by (4.2). The starting set of differential equations (4.1) can be re-written using the circuit variables gained after the synthesis process into a dimensional form. This is useful when we want to check if our realization corresponds with the mathematical model. Let u_1 be the voltage across capacitor C_1, u_2 the voltage across C_2 and i the current through L. Using the standard method of modal voltages and junction currents the following can be written:

$$\begin{aligned} C_1 \cdot \frac{du_1}{dt} &= \frac{u_2 - u_1}{R_1} - f(u_1), \\ C_2 \cdot \frac{du_2}{dt} &= \frac{u_1 - u_2}{R_1} - i, \\ L \cdot \frac{di}{dt} &= u_2 - iR_2. \end{aligned} \tag{4.14}$$

This form of description is also widely used, especially for chaotic systems that did not come first from a purely mathematical model.

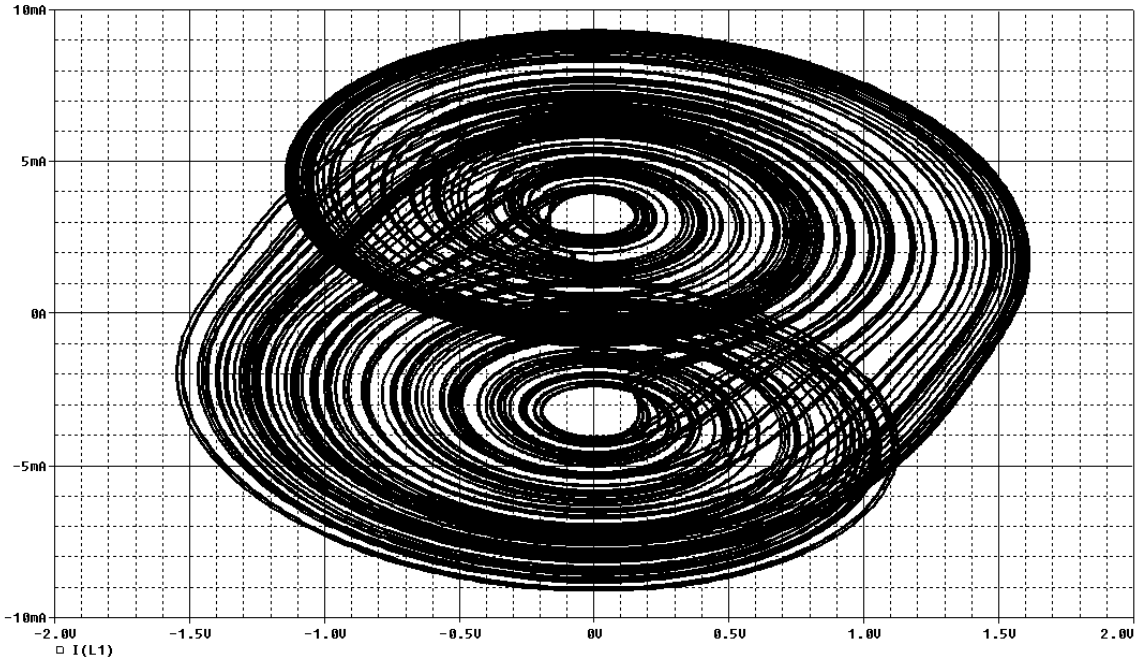

Figure 4.2 Simulated attractor of the Chua circuit. Plotting u_1 vs i.

Simulating the circuit on Figure 1.1 using component ORCAD PSpice, a chaotic behavior can be observed with the following values: R_1 = 100 Ω , R_2 = 100 Ω, R_3 = 1 kΩ, R_4 = 22 kΩ, R_5 = 22 kΩ, R_6 = 1 kΩ, R_7 = 900 Ω , R_8 = 1 Ω , C_1 = 680 pF, C_2 = 6,8 nF, L = 1 mH. The chaotic attractors are depicted on Figure 4.2 and Figure 4.3 and have the pattern of a double scroll, typical of the Chua circuit.

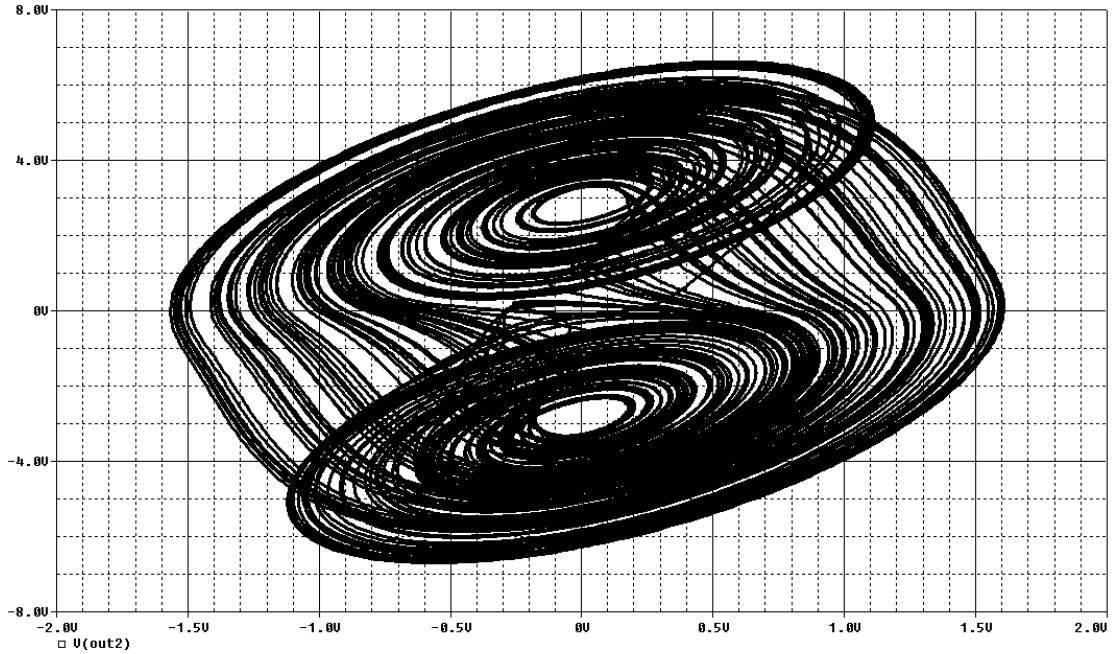

Figure 4.3 Simulated attractor of the Chua circuit. Plotting u_1 vs u_2.

4.2 Integrator block diagrams

Another method of synthesizing circuits from differential equations is by using block diagrams. This method was historically used in great extent to simulate dynamic systems using analog computers [29]. This method will in general create more complex circuit realizations than classical synthesis but will always lead to a solution. Figure 4.4 shows how (4.1) can be drawn as a block diagram. Turning the diagram into an electrical circuit can be done in multiple ways, depending on what components we have available. In this case a summing inverting integrator and summing inverter will be used.

The block diagram on Figure 4.4 can be the re-drawn into Figure 4.5, from which the electrical circuit can be synthesized, using the mentioned building blocks, which

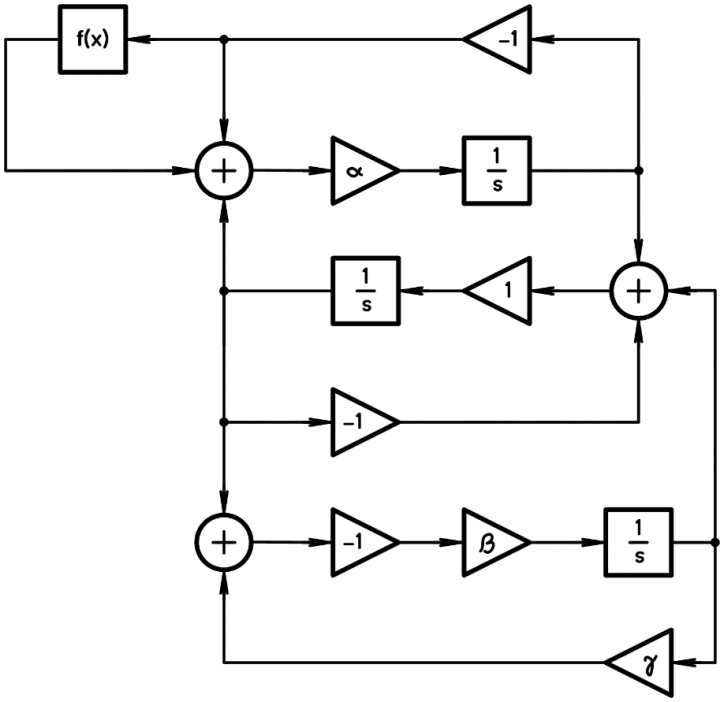

Figure 4.4 Block diagram of the Chua circuit.

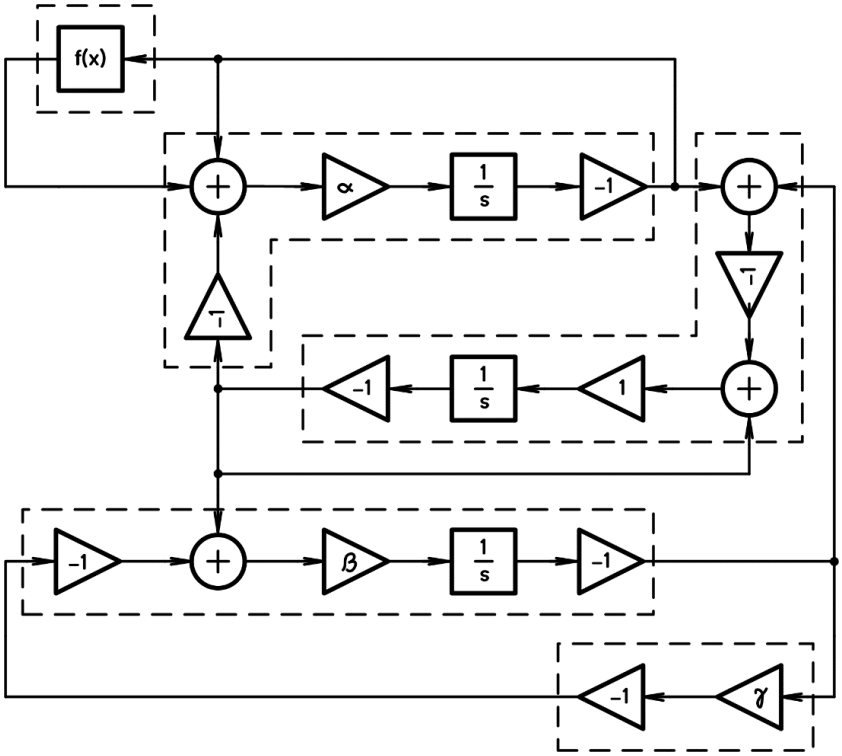

Figure 4.5 Modified block diagram of the Chua circuit.

are also displayed on Figure 4.6. The non-linear function *f(x)* can be realized by two pairs of biased diode limiters and several summing inverters.

The final circuit is displayed on Figure 4.7. In comparison to the previous method this realization is, as predicted, much more complex and contains a large number of active elements. In this circuit integration of dx/dt *is* performer by B_1, where the

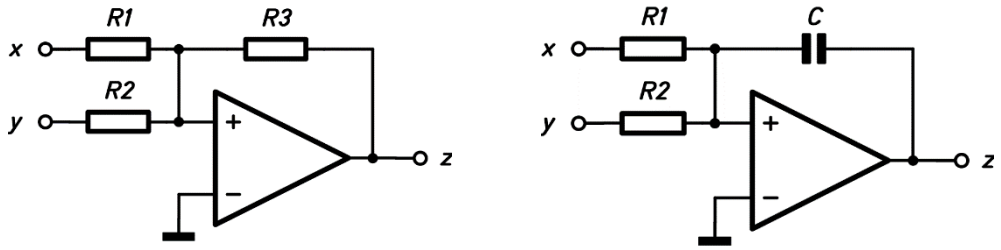

$$z = -\frac{R_3}{R_1} \cdot x - \frac{R_3}{R_2} \cdot y \qquad z = -\int_0^t \left(\frac{1}{R_1 C} \cdot x + \frac{1}{R_2 C} \cdot y\right) dt$$

a) b)

Figure 4.6 Schematic diagram and function equation of a) summing inverter b) summing integrator.

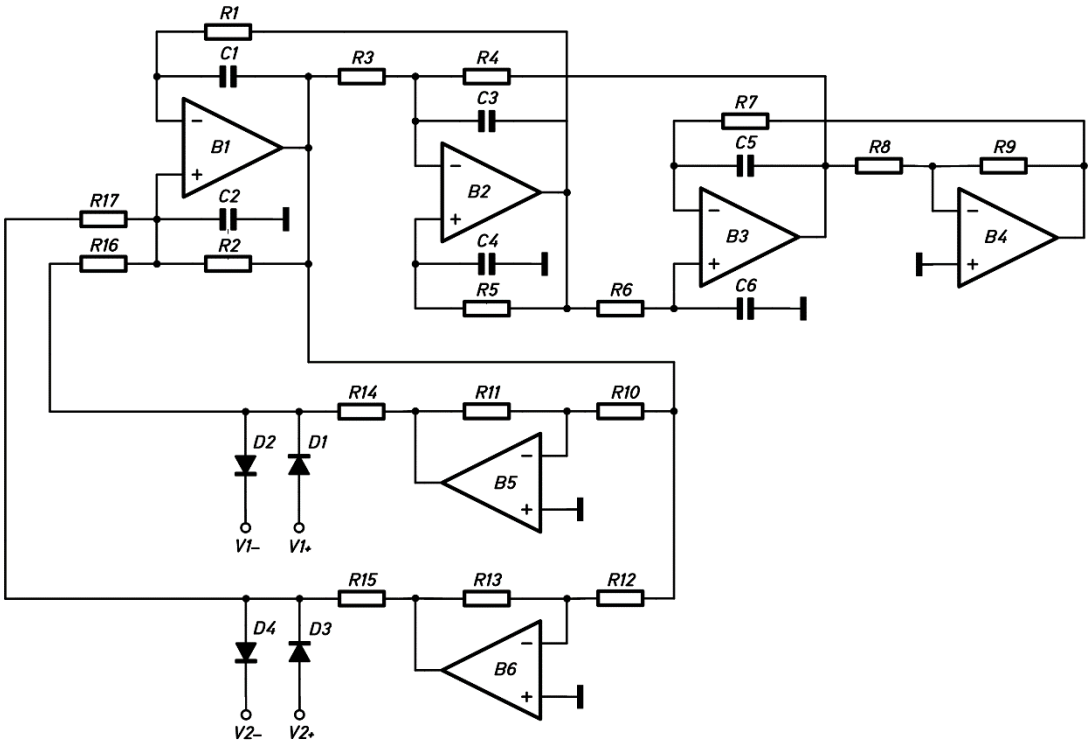

Figure 4.7 Schematic diagram of the synthesized Chua chaotic circuit

constant α is set by the value of capacitors C_1 and C_2 and their accompanying resistors. The integration constant of dy/dt is 1, however can be scaled with the rest of the circuit to obtain practical signal variable values. The β variable is set by

capacitors C_5 and C_6 and their accompanying resistors. The γ constant is then realized by the gain of amplifier B_4. Both inverting and non-inverting summing is performed to minimalize the needed number of active elements. The non-linear function (4.2) is realized by the amplifiers B_5 and B_6, with diodes D_1 to D_4. The breakpoints of the PWL function are determined by the threshold voltage of the diodes, plus the connected reference voltages. If this circuit was to be built and tested, simple voltage dividers from the supply voltages would most likely be best suited for this task. The constants *a* and *b* are determined by gain of the amplifiers B_5 and B_6. The voltage transfer function is depicted on Figure 4.8, obtained from PSpice simulation.

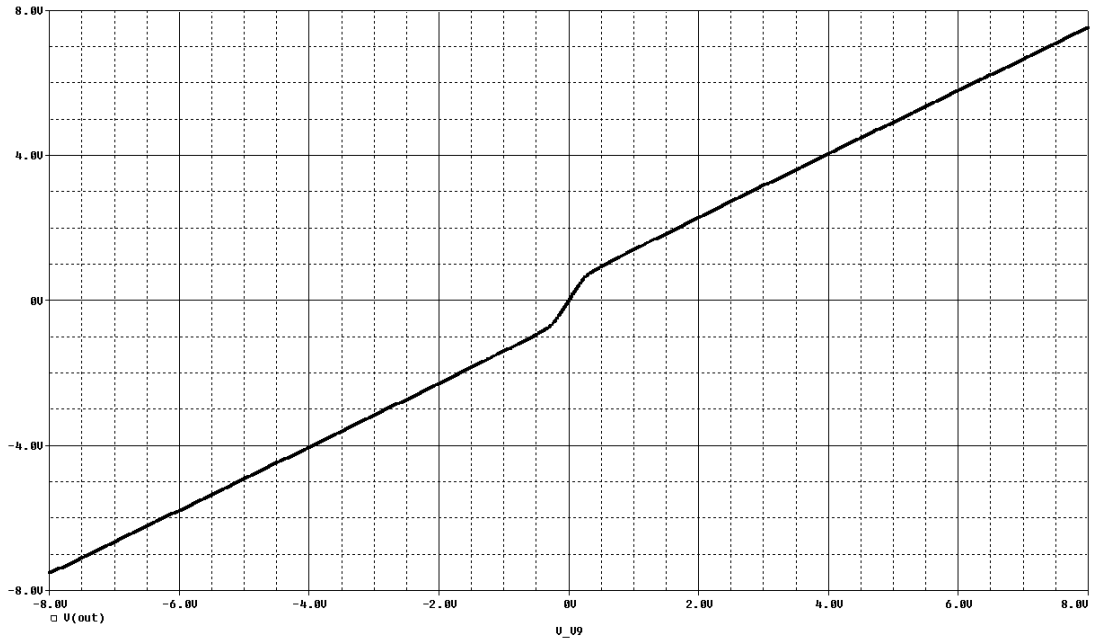

Figure 4.8 Transfer characteristic of the non-linear PWL function.

5. FRACTAL CHAOTIC CIRCUIT

This chapter describes design and simulation of the fractal chaotic system. As mentioned, first, an integer order chaotic system will be synthesized and then, by substituting some of the capacitors by fractal capacitors, a fractal chaotic system will be created. The integer order system chosen is of the 4th order and is described as

$$\begin{aligned} C_1 \cdot \frac{du_1}{dt} &= (-i_1 - gm_2(u_2)), \\ L_1 \cdot \frac{di_1}{dt} &= u_1, \\ C_2 \cdot \frac{du_2}{dt} &= (-i_2 - gm_1(u_1)), \\ L_2 \cdot \frac{di_2}{dt} &= u_2. \end{aligned} \tag{5.1}$$

Where gm_1 and gm_2 are two non-linear cubic polynomial functions

$$gm_2 = a_1 \cdot {u_2}^3 - b_1 \cdot u_2, \qquad gm_1 = a_2 \cdot {u_1}^3 - b_2 \cdot u_1. \tag{5.2}$$

5.1 Circuit design

A circuit realization of the system described by (5.1) is depicted on Figure 5.1. The circuit consists of two resonant LC circuits cross-coupled by two non-linear transconductances.

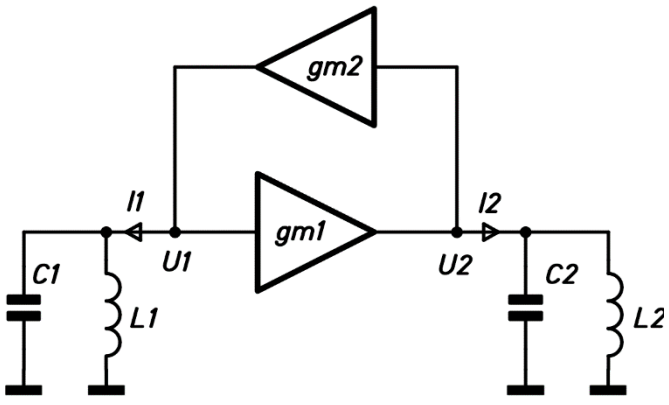

Figure 5.1 Simplified schematic diagram of the 4th order chaotic circuit.

The two non-linear transconductances were realized using a combination of AD633 analog multipliers [30] and TL072 operational amplifiers [31]. The schematic

representation of these two transconductances is depicted on Figure 5.2 and Figure 5.3.

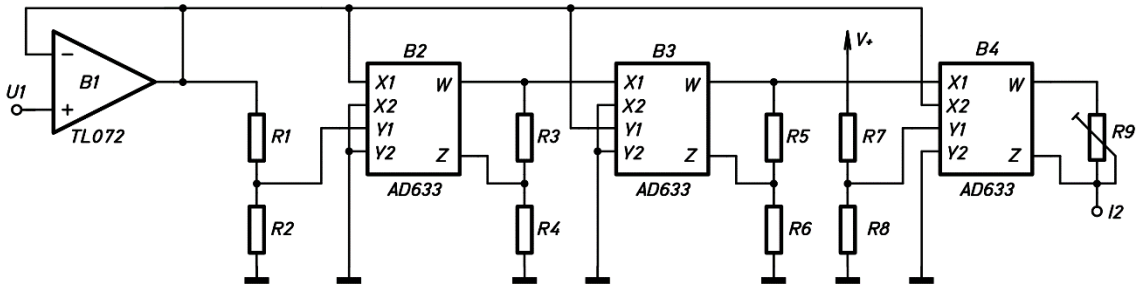

Figure 5.2 Schematic diagram of the non-linear transconductance gm_1.

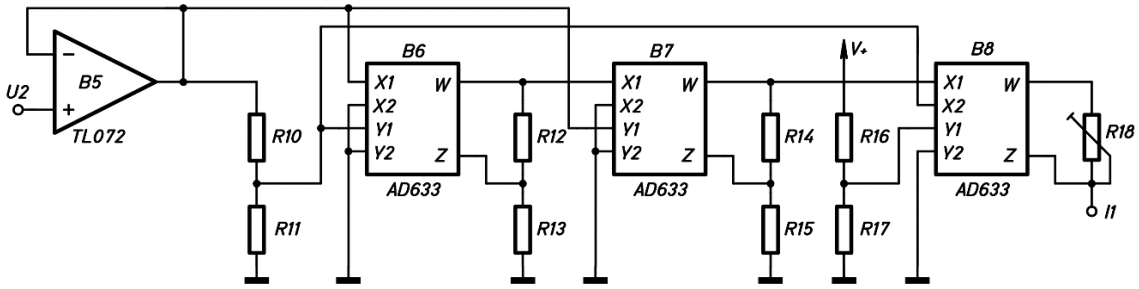

Figure 5.3 Schematic diagram of the non-linear transconductance gm_2.

The AD633 is a 4-quadrant analog multiplier and it's behavior is described by

$$U_W = 0{,}1 \cdot (U_{X1} - U_{X2}) \cdot (U_{Y1} - U_{Y2}) + U_Z. \tag{5.3}$$

In the circuit on Figure 5.3 Schematic diagram of the non-linear transconductance *gm2*. and Figure 5.3, the B_1 is used as a buffer, the two voltage dividers are used for scaling, and to increase the dynamic range of the system. Next, the analog multiplier B_2 realizes the function x^2, which is further multiplied by the next AD633 to realize the cubic function. The last AD633 is used as a summing amplifier and provides voltage to current conversion.

Simulating the above circuit in PSpice, it can be observed that the circuit closely resembles the precise mathematical function, with some offset error present. Notable is the fact that the circuit saturates at around 3 V on one node and 4,5 V on the other one. For the system equations to stay valid, the attractor must fit within this voltage range. Values for a and b constants were selected for gm_1 and gm_2, according to available mathematical model in which chaos was observed. The transfer functions gm_1 and gm_2 are plotted on Figure 5.4 and Figure 5.5.

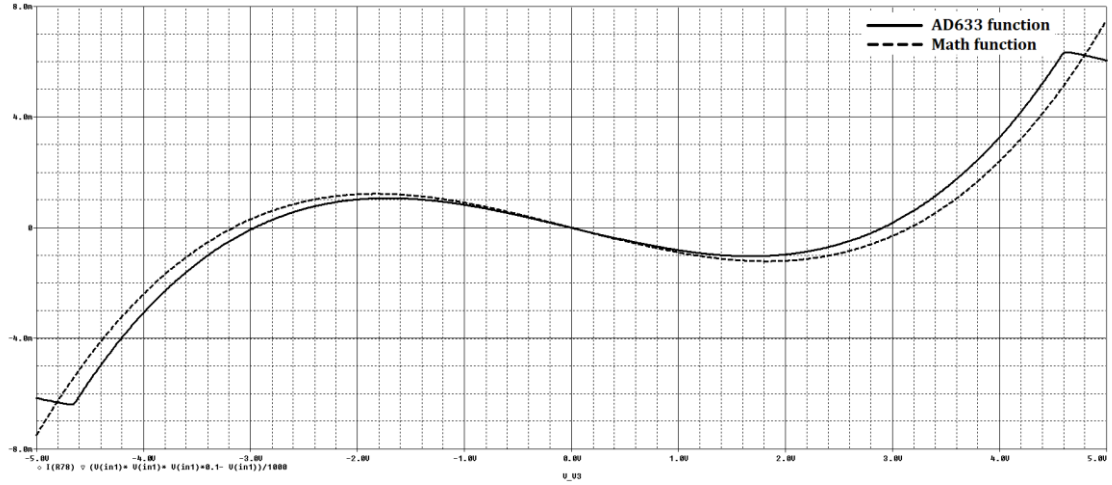

Figure 5.4 Transfer characteristic of the non-linear transconductance gm_1.

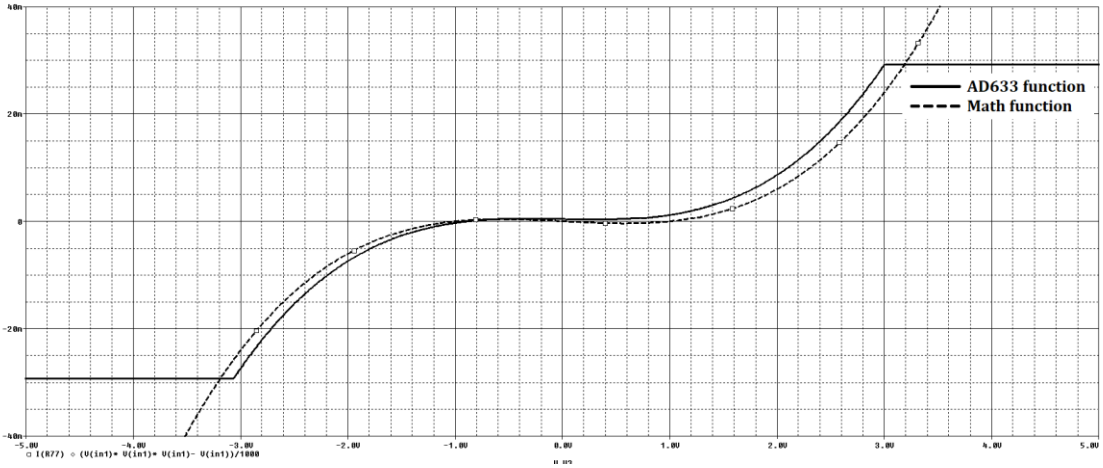

Figure 5.5 Transfer characteristic of the non-linear transconductance gm_2.

Realizing the dynamic system as an electrical circuit requires the time-dependent variables to be scaled down to levels, which the circuit can handle without distortion. The time constant must also be multiplied so that attractors can be measured in a timely manner and also so the fractal capacitors designed in the previous chapter can be used. In the chaotic system described by (5.1) and (5.2), chaos was observed with constants $C_1 = C_2 = 1$, $L_1 = L_2 = 1$, $a_1 = 0{,}1$, $a_2 = 1$ and $b_1 = b_2 = 1$ with the time constant equal to 1. The time variable constants are to be transformed according to

$$L = \frac{L_n \cdot \zeta_n}{\omega_n} \qquad C = \frac{C_n}{\omega_n \cdot \zeta_n}, \tag{5.4}$$

where L and C are the transformed inductance and capacitance, L_n and C_n are the normalized values, ω_n is the frequency scaling factor, given as $\omega_n = \omega_0/\Omega$ where

ω_0 is the desired angular frequency and Ω is the frequency norm, and ζ_n is the impedance scaling factor, given as $\zeta_n = Z_0/\zeta$ where Z_0 is the desired impedance and ζ is the impedance norm.

Scaling the impedance up will decrease the currents in the circuit and scaling the frequency up will change the values of capacitors and inductors to more reasonable values. To be able to use all 3 of the fractal capacitors designed in the first chapter, it is necessary to set the scaling factors so that the circuit will operate in the intersection point visible in Figure 2.4. The impedance norm was therefore set to 1 kΩ and the frequency norm was set to 4,823 kHz. This yields L = 33 mH and C = 33 nF, which are reasonable values for these components, and the impedance norm will decrease the currents in the circuit by a factor of 1000, down to milliamperes. Verifying the resonance in SPICE simulation shows, that both the integer order resonant circuit and the fractional ones operate at the correct frequency.

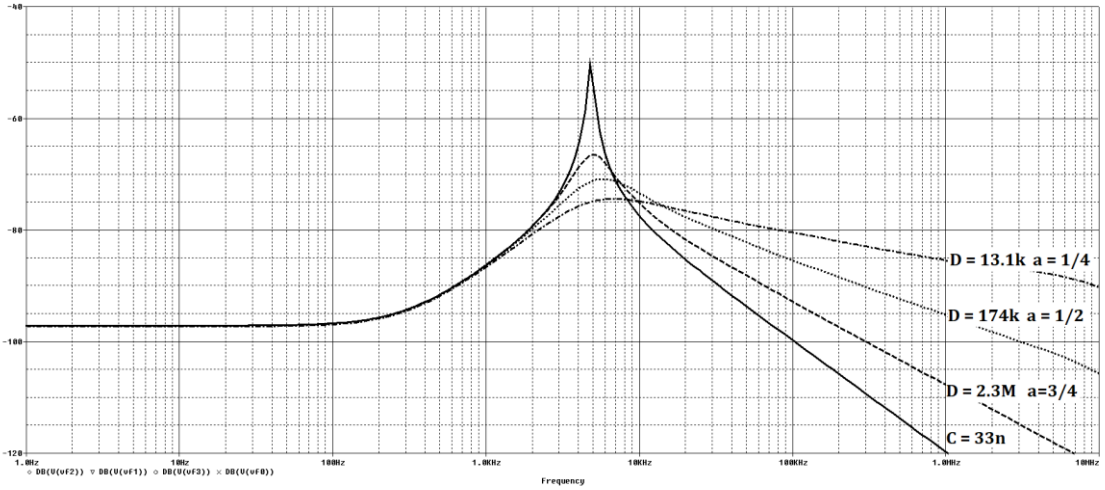

Figure 5.6 Simulation of the resonant frequency of the integer and fractal order circuit.

The inductor that is to be used in the circuit is from the RL8010 series by the manufacturer MATSUTA with nominal DC resistance of 70 Ω, which was measured at 65 Ω for the purchased units. This value will have impact on operation of the chaotic circuit and must be compensated for. That is why in the Figure 5.3 Schematic diagram of the non-linear transconductance gm_2. and Figure 5.3, the scaling resistors R_9 and R_{18} are made variable. The mathematical model of the chaotic circuit can also be modified to reflect the DC resistance of the inductors, for more accurate numerical analysis. This modified system of differential equations is as follows:

$$
\begin{aligned}
C_1 \cdot \frac{du_1}{dt} &= -i_{L1} - gm_2(u_2), \\
L_1 \cdot \frac{di_1}{dt} &= u_1 - R_{L1} \cdot i_1, \\
C_2 \cdot \frac{du_2}{dt} &= -i_{L2} - gm_1(u_1), \\
L_2 \cdot \frac{di_2}{dt} &= u_2 - R_{L2} \cdot i_2.
\end{aligned}
\tag{5.5}
$$

5.2 Simulation of the integer order system

As with all other circuits in this thesis, the chaotic system was simulated in PSpice. With a lossless inductor, chaotic behavior depicted on Figure 5.7 was observed. Looking at the spectral data, a clear peak at the resonant frequency of the LC network is visible, as well as few more at 5 kHz and near 14 kHz.

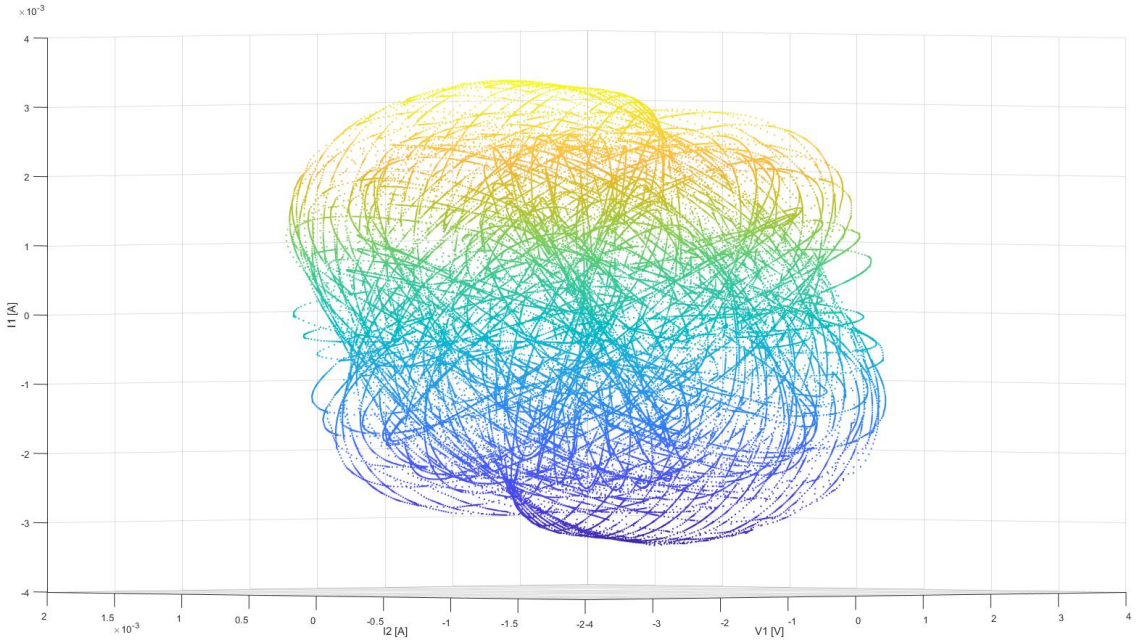

Figure 5.7 Chaotic behavior of the circuit with lossless inductor. Plotted is the relationship between U_1, I_1 and I_2.

Now, that chaos is confirmed in the circuit, the next step is to evaluate the behavior when lossy inductors are present. When simulating the circuit with lossy inductors, the chaotic behavior disappears. However, if the gain of the two non-linear

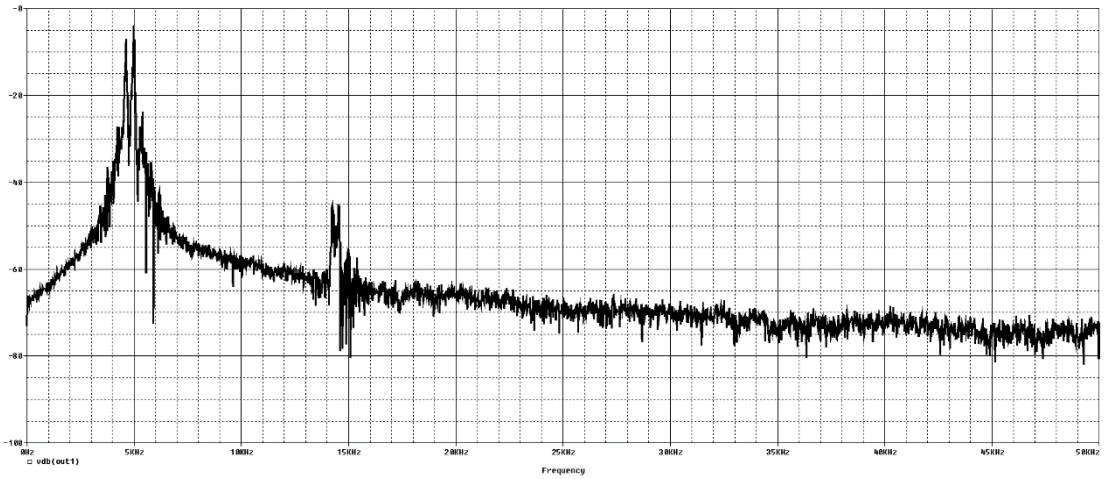

Figure 5.9 Spectral analysis of the voltage at U_1 of the circuit with the ideal inductor.

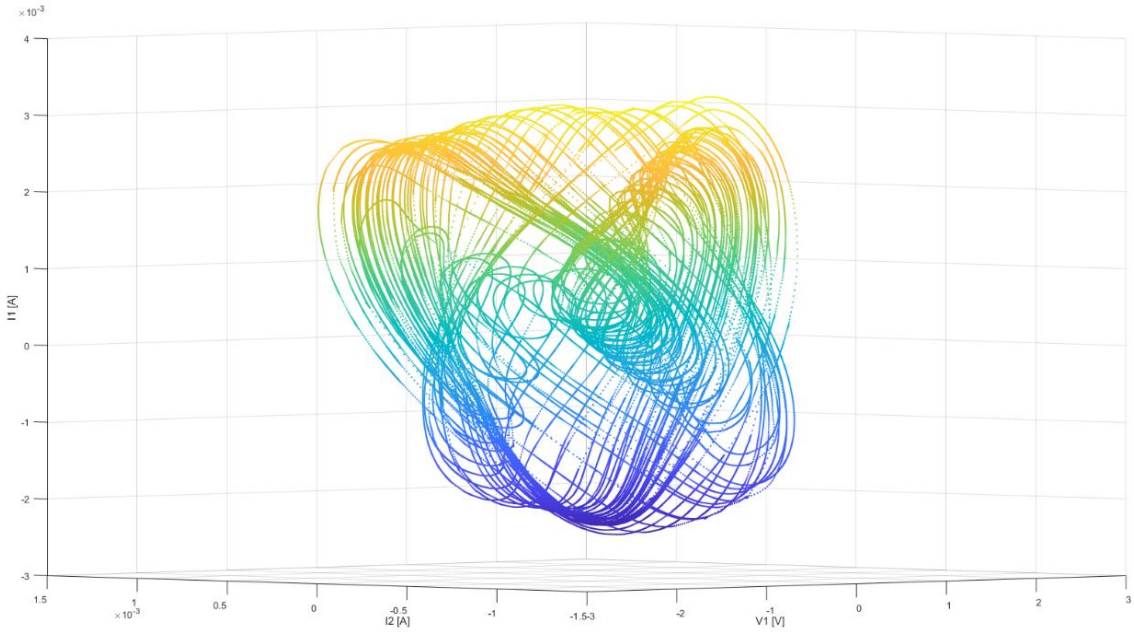

Figure 5.8 Chaotic behavior of the circuit with lossy inductor. Plotted is the relationship between U_1, I_1 and I_2.

transconductances is adjusted, to compensate for the now finite Q factor, the chaos will re-appear and we can observe further. Figure 5.8 and Figure 5.11 depict attractors obtained from the new, modified circuit. The newly obtained attractors

have a different shape from the ones with the lossy inductor, this circuit can be however actually verified with real world measurements, which will also be done later. Looking at the spectral data it is richer in harmonic content, both odd and even. The fundamental frequency of the resonant circuit is not present anymore, instead the most dominant peak is at 6,4 kHz with one below, and many above.

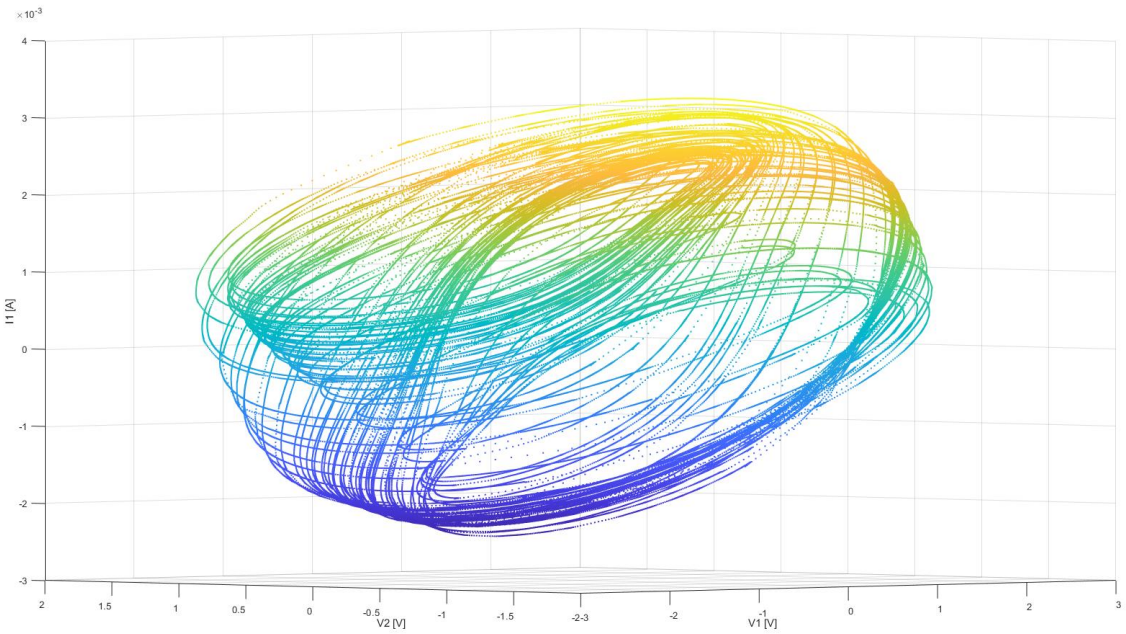

Figure 5.11 Chaotic behavior of the circuit with lossy inductor. Plotted is the relationship between U_1, U_2 and I_2.

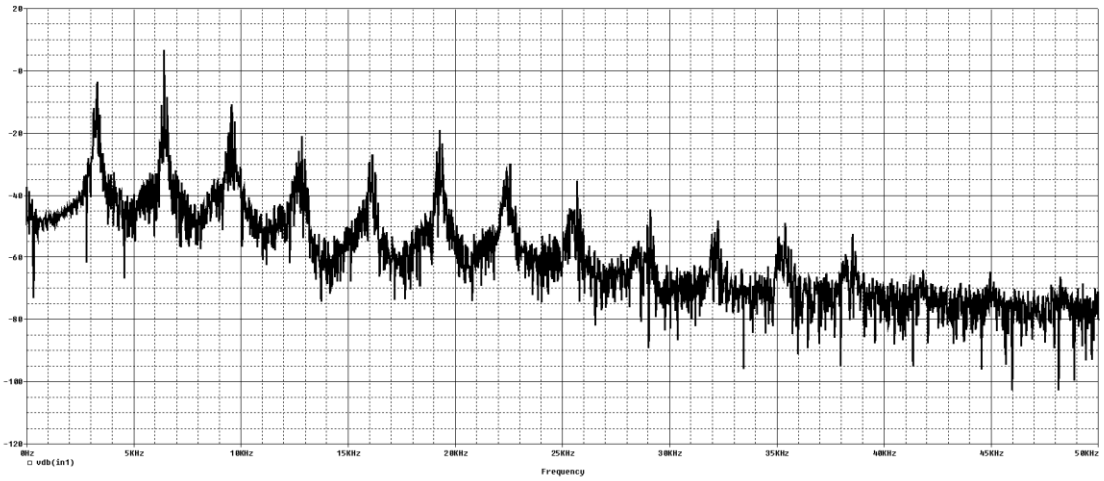

Figure 5.10 Spectral analysis of the voltage at U_1 of the circuit with lossy inductors.

5.3 Simulation of the fractal order system

The circuit on Figure 5.1 can be made into fractal order by substituting one of the capacitors C_1 or C_2 by a fractal capacitor approximation, one that was synthesized in the Chapter 2. This circuit will be the subject of interest for testing properties of fractal order chaotic circuits. It is displayed on Figure 5.12.

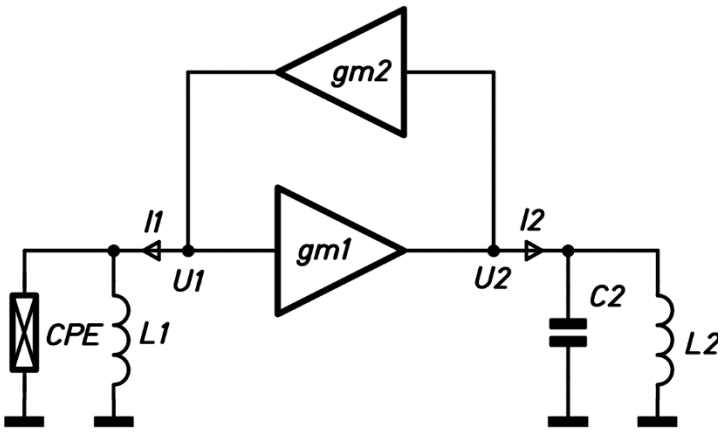

Figure 5.12 Simplified diagram of the fractal chaotic circuit.

Without any modifications to the circuit, the chaotic behavior disappears. This is with accordance with the hypothesis presented in Chapter 3.2, for decreasing value of α it is necessary to increase the gain further to facilitate the chaotic behavior. Increasing the gain for each individual circuit variation accordingly, the chaos will re-appear, and a different set of attractors can be observed. Looking at the spectral

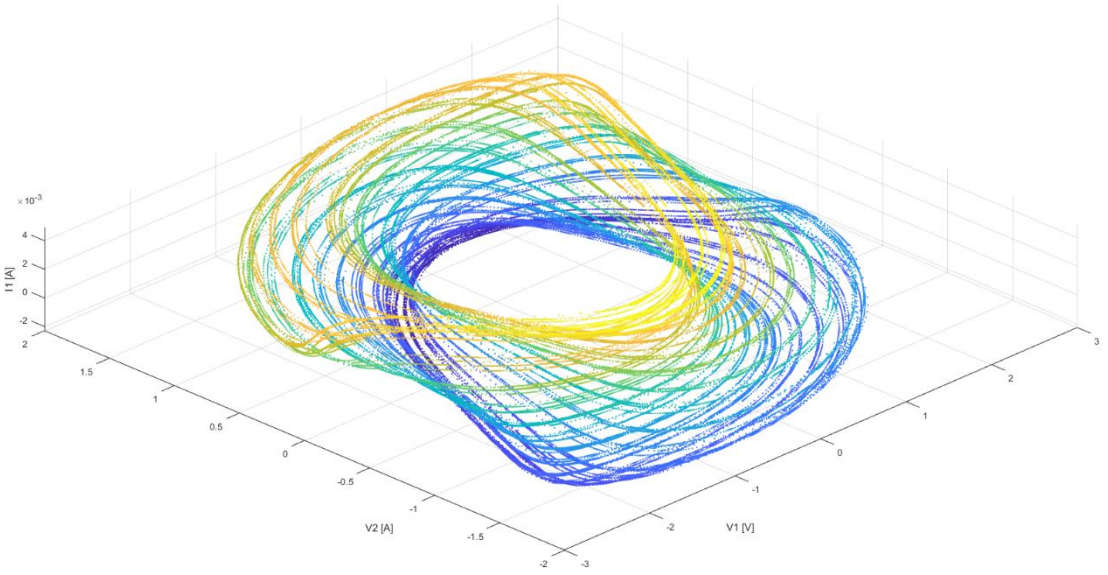

Figure 5.13 Chaotic behavior of the circuit with lossy inductor and C_2 fractal capacitor with $\alpha = ¾$. Plotted is the relationship between U_1, U_2 and I_2.

data we again can observe unique behavior for each of the circuit variations, with varying spectral content. Both capacitors, C_1 and C_2 can be substituted, and the resulting attractors are different in each case. Only when C_1 being fractal with α = ¾ chaos didn't appear.

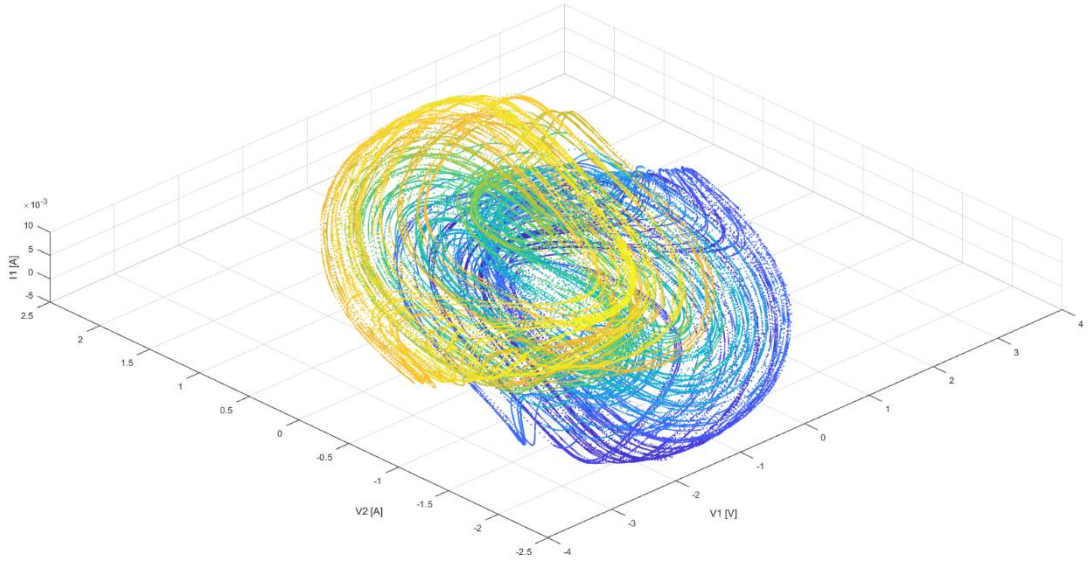

Figure 5.14 Chaotic behavior of the circuit with lossy inductor and C_2 fractal capacitor with α =½ . Plotted is the relationship between U_1, U_2 and I_2.

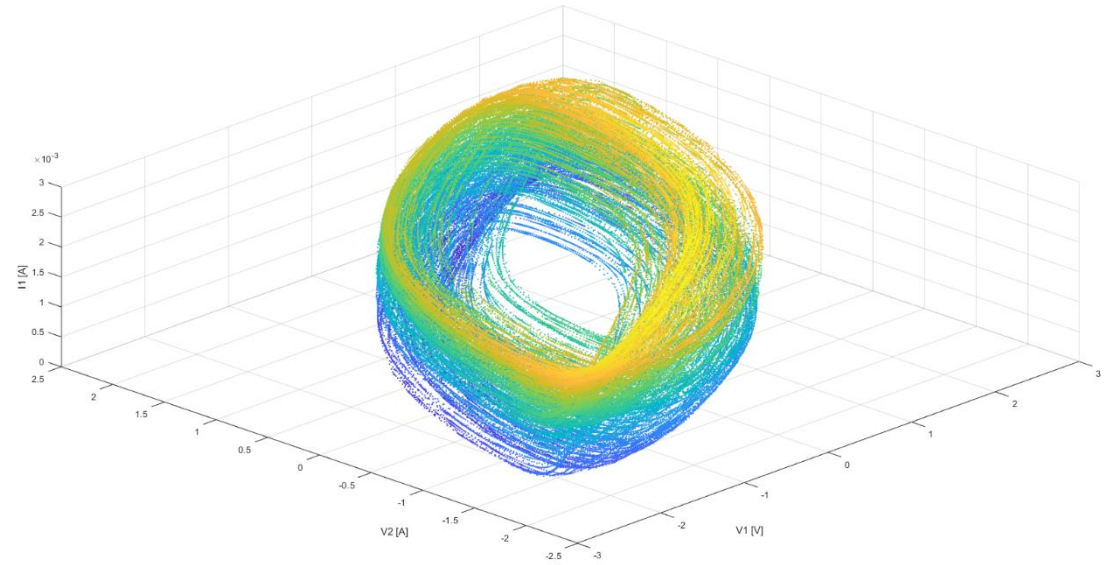

Figure 5.15 chaotic behavior of the circuit with lossy inductor and C_2 fractal capacitor with α = ¼. Plotted is the relationship between U_1, U_2 and I_2.

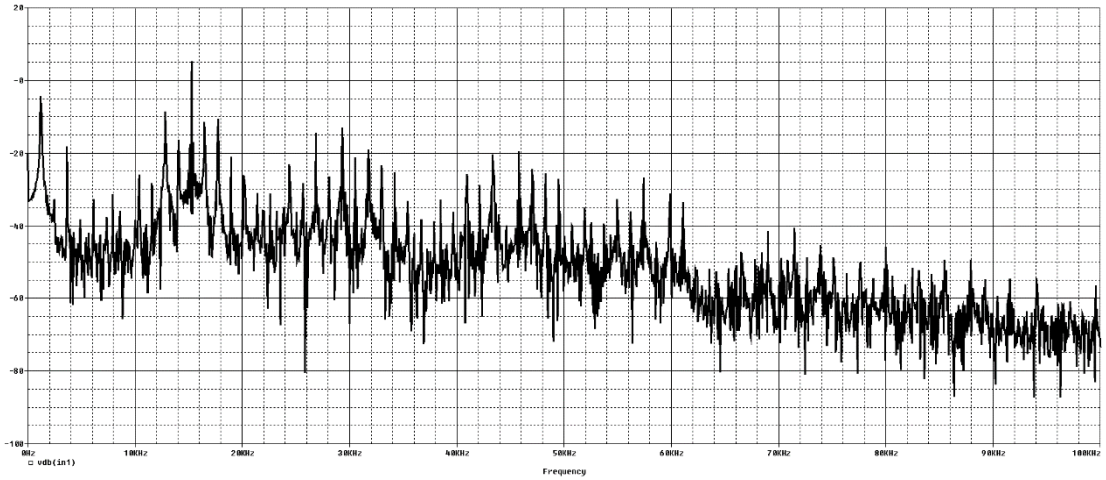

Figure 5.16 Spectral analysis of the voltage at U_1 of the circuit with the lossy inductor and fractal capacitor with α = ¼.

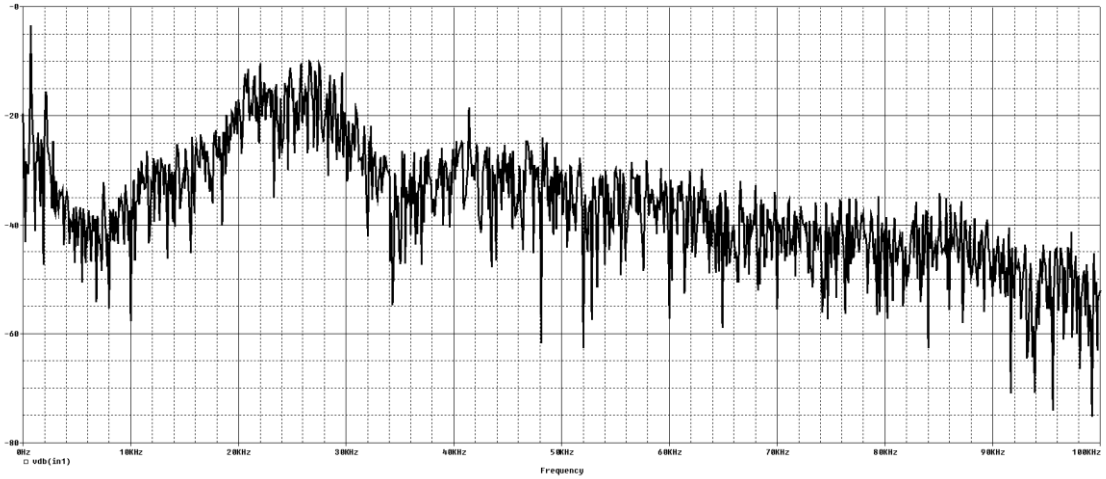

Figure 5.17 Spectral analysis of the voltage at U_1 of the circuit with the lossy inductor and fractal capacitor with α = ½.

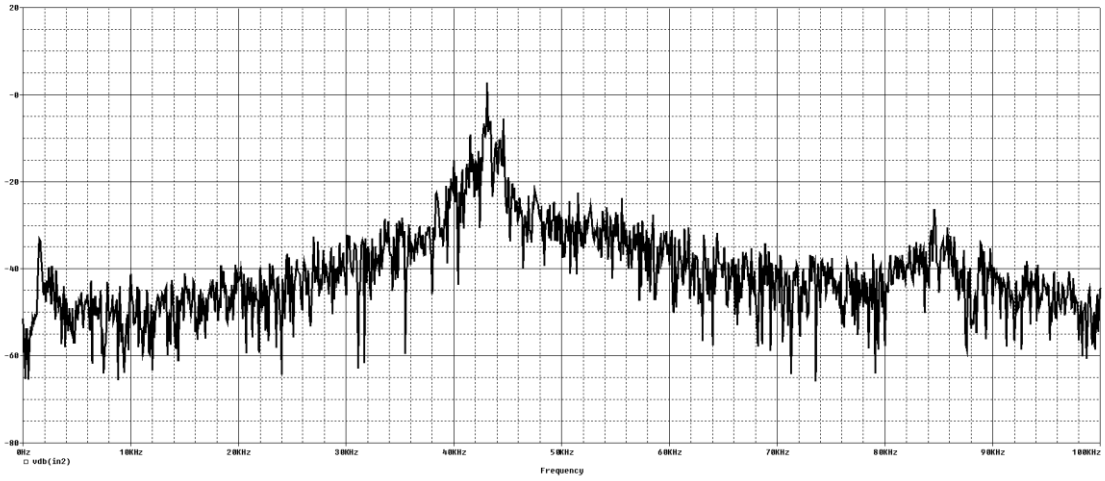

Figure 5.18 Spectral analysis of the voltage at U_1 of the circuit with the lossy inductor and fractal capacitor with α = ¾.

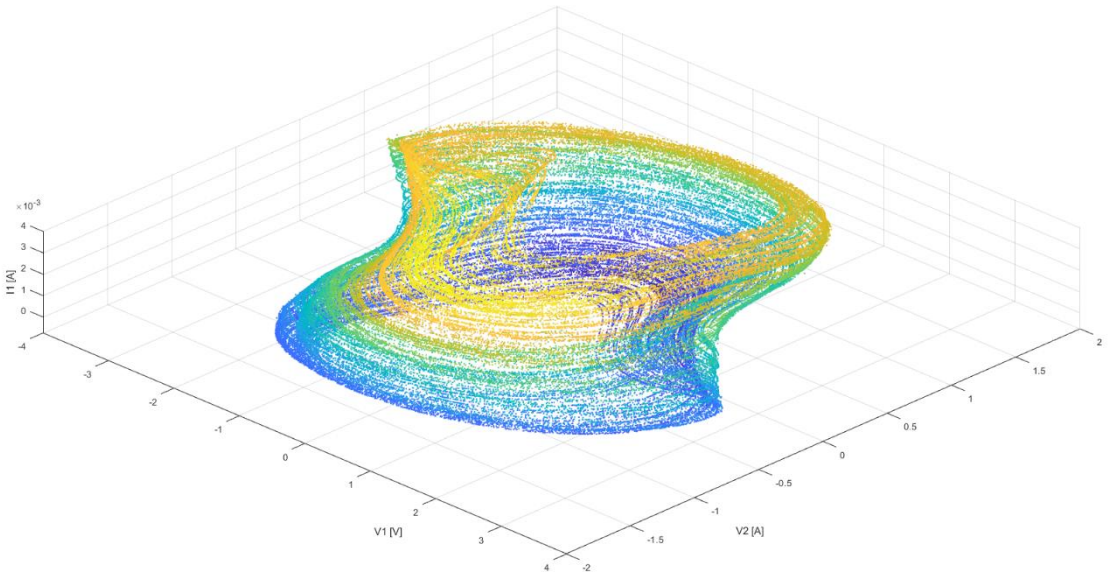

Figure 5.19 Chaotic behavior of the circuit with lossy inductor and C_1 fractal capacitor with α =½. Plotted is the relationship between U_1, U_2 and I_2.

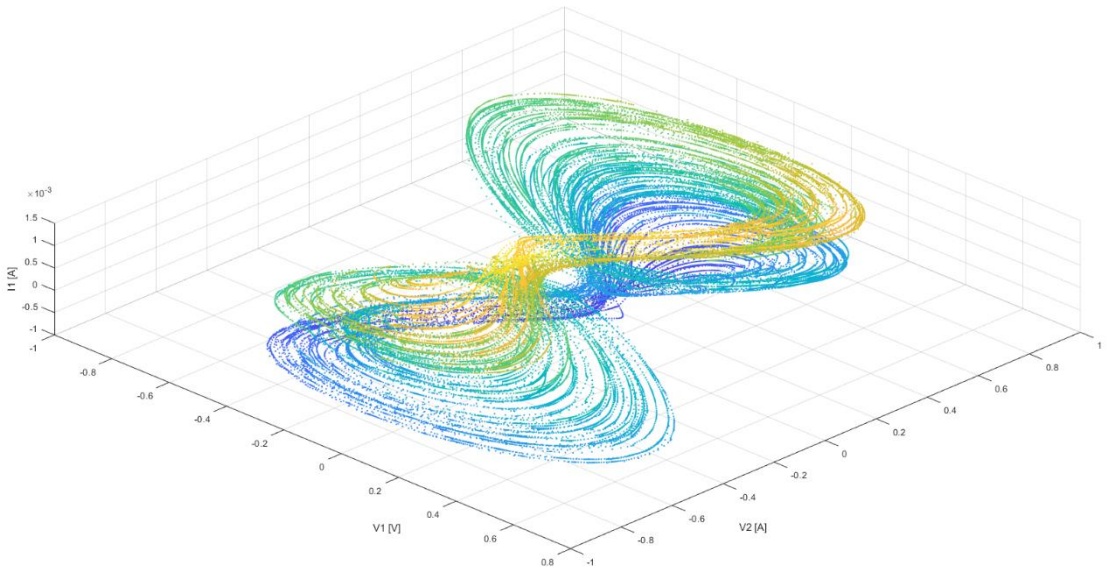

Figure 5.20 Chaotic behavior of the circuit with lossy inductor and C_1 fractal capacitor with α =¼. Plotted is the relationship between U_1, U_2 and I_2.

6. VERIFICATION

This chapter deals with verification of the simulated attractors observed in the designed circuit. The constructed prototype of the circuit, utilizing the prepared CPE elements will be measured and the results discussed. Finally, a mathematical model of the circuit will be constructed, and numerical analysis will be performed.

6.1 Real life measurements

The designed circuit was first manufactured in form of a printed circuit board, with THT components. The section containing the frequency dependent passive elements was made with sockets, so the fractal elements can be swapped-in for regular capacitors and vice versa according to need. The PCB layout and component list is available in the appendix section. The resistors setting the current gain of B4 and B8 were made variable as multi-turn trimmers. The measurement was performed as follows: First, the desired combination of passive time-variant elements was inserted into the circuit, then with the help of the two trimmers gain was adjusted, so that chaos was present in the circuit. Those values were then written down, so that the circuit could be accurately analyzed numerically. Waveforms were displayed in the XY mode of a digital oscilloscope, voltage variables directly, while the current through the inductor was measured with a small shunt resistor. Waveforms were captured using a HP 54624A oscilloscope. Despite the fact that the sampling rate of the oscilloscope is low, the attractors are well visible, and comparisons can be made with the graphs obtained through simulation. Figure 6.1 and Figure 6.2 shows the captured attractor of the circuit of integer order with foil capacitors, the shunt value of the resistor was 4,7 Ω, so the y axis displays the current with about 5 times magnification in respect to the oscilloscope scale. This value was chosen as a good compromise between how much the added resistance changes the properties of the circuit and the amount of detail that can be captured, before noise starts to interfere with the attractor pattern.

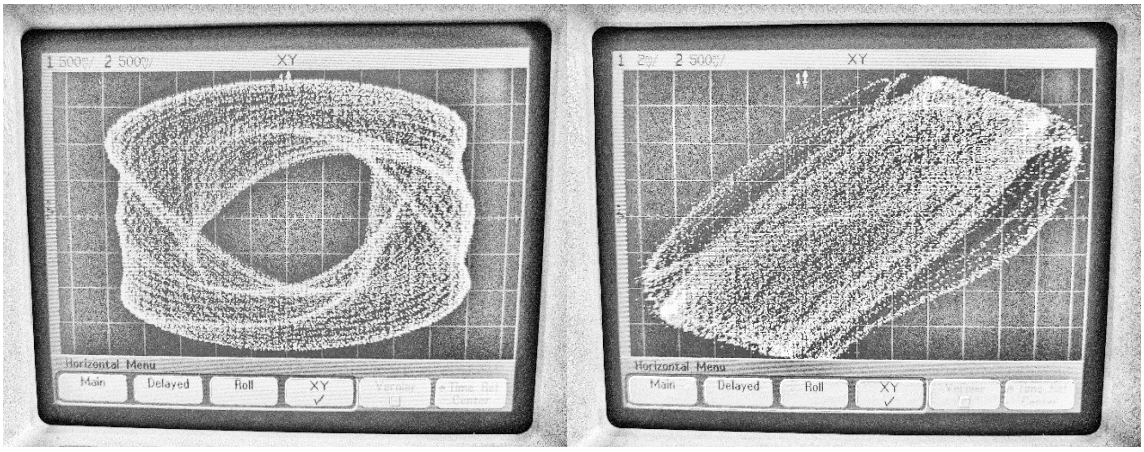

Figure 6.1 a) Measured chaotic attractor U_1 vs. U_2 and b) I_1 vs U_2 from the integer order system.

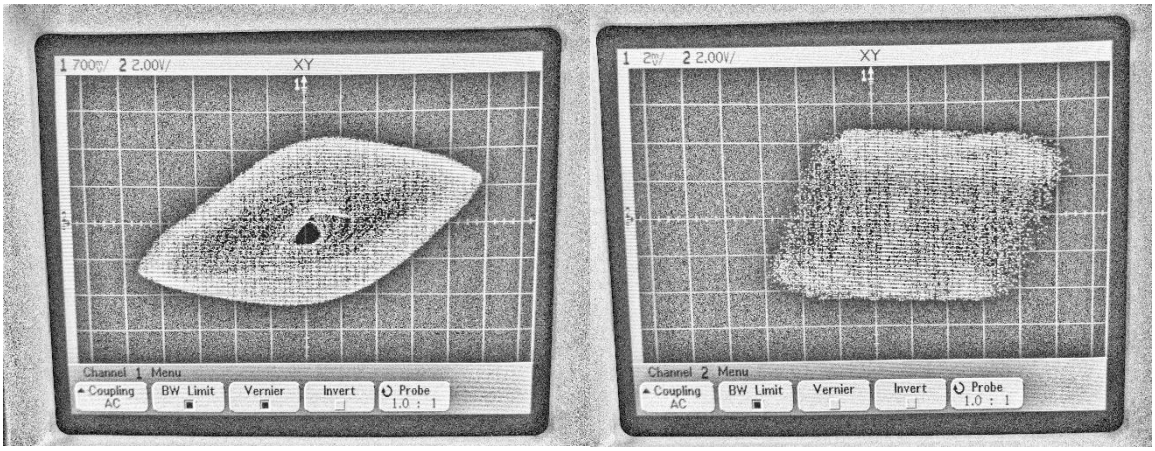

Figure 6.2 a) Measured chaotic attractor U_1 vs. U_2 and b) I_1 vs U_2 from the fractal order system with C_2 fractal capacitor and α = ¼.

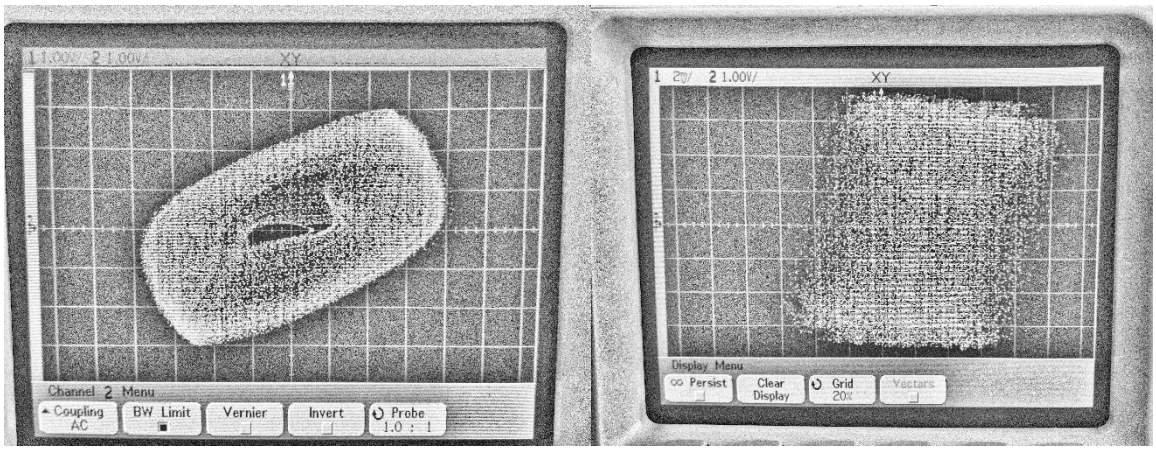

Figure 6.3 a) Measured chaotic attractor U_1 vs. U_2 and b) I_1 vs U_2 from the fractal order system with C_2 fractal capacitor and α =½.

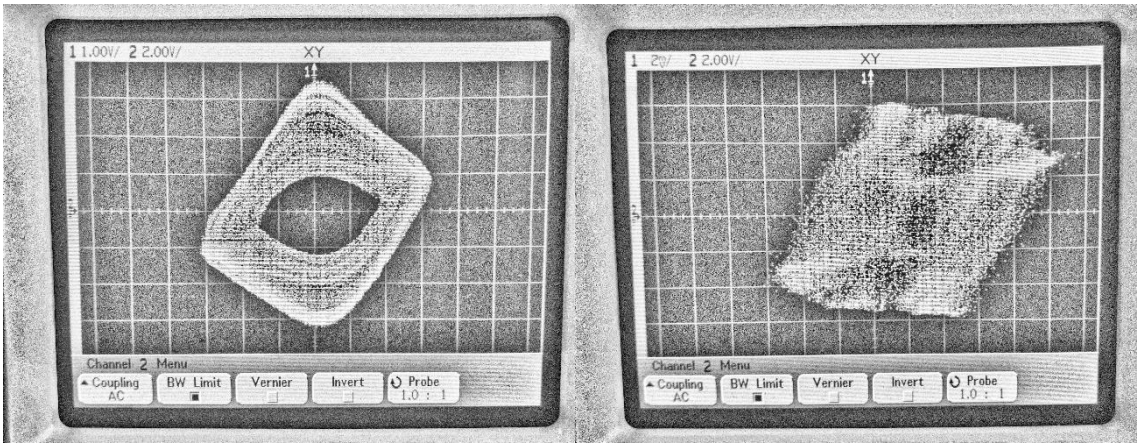

Figure 6.4 a) Measured chaotic attractor U_1 vs. U_2 and b) I_1 vs U_2 from the fractal order system with C_2 fractal capacitor and α=¾.

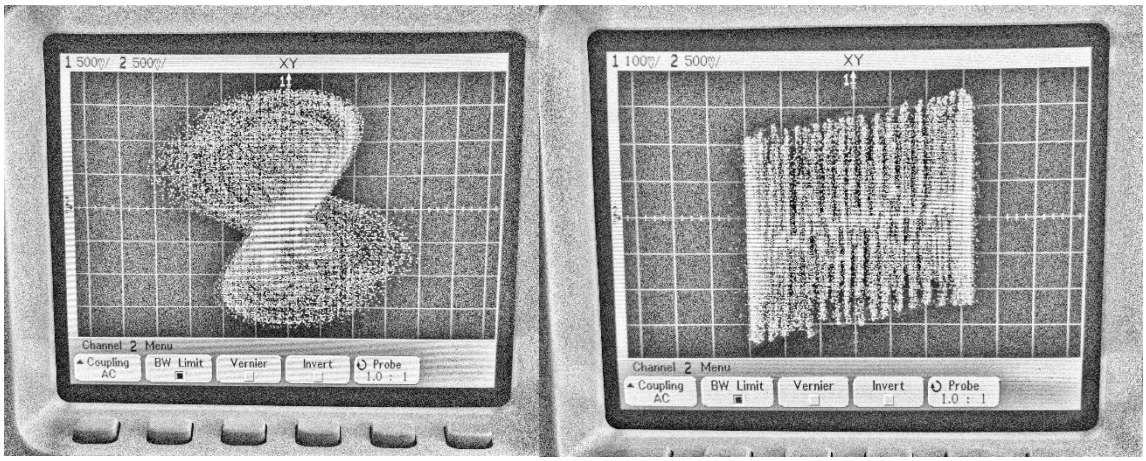

Figure 6.5 a) Measured chaotic attractor U_1 vs. U_2 and b) I_1 vs U_2 from the fractal order system with C_1 fractal capacitor and α = ¼.

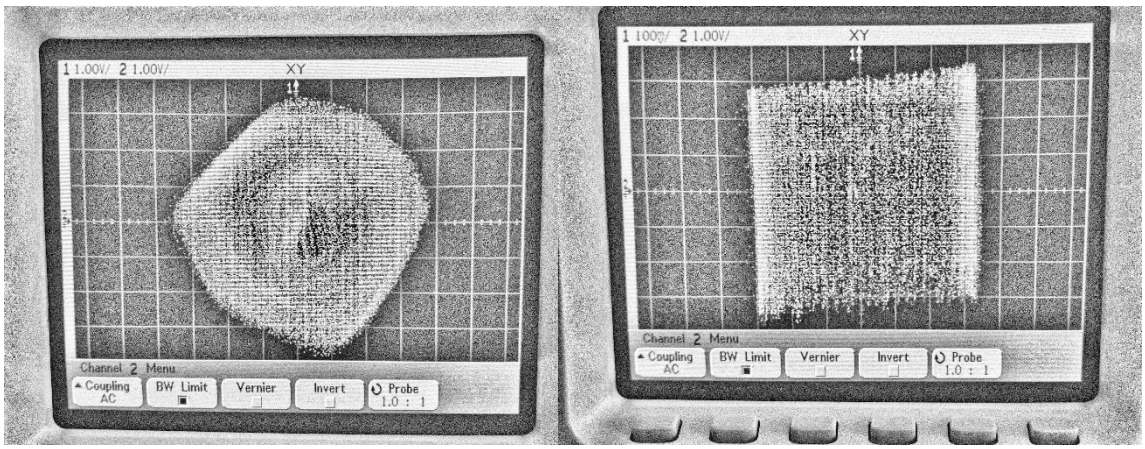

Figure 6.6 a) Measured chaotic attractor U_1 vs. U_2 and b) I_1 vs U_2 from the fractal order system with C_1 fractal capacitor and α = ½.

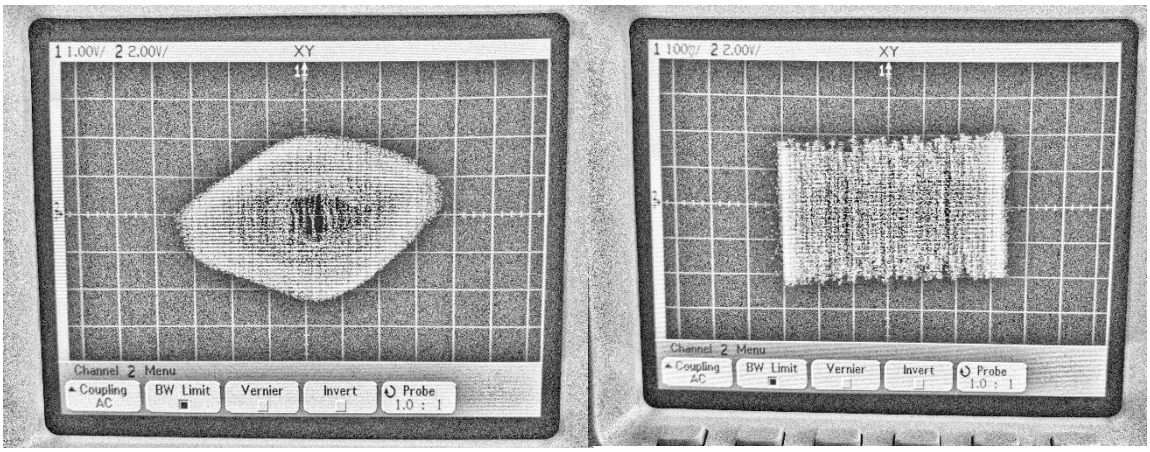

Figure 6.7 a) Measured chaotic attractor U_1 vs. U_2 and b) I_1 vs U_2 from the fractal order system with C_1 fractal capacitor and α = ¾.

From the measured data, a few observations can be made. The integer order chaotic system matches the simulated results quite precisely. It can therefore be claimed that the simulated circuit represents the physical realization accurately. There is a close resemblance between the measured attractors of the fractional order systems and the simulated ones, namely Figure 6.5 and Figure 5.20 which show the same situation are very close match. Figure 6.2 to Figure 6.4 also match the change in shape that can be observed on Figure 5.15 to Figure 5.12. There are, however, some differences clearly visible from the oscilloscope screenshots, namely Figure 6.4 being perhaps the least accurate. Furthermore, the circuit variation when the capacitor C_1 is fractal with α = ¾ it was possible to detect chaotic behavior, but proven not possible to simulate, due to the transition from harmonic oscillation to instability being too sensitive. The described discrepancies can be attributed to non-precise setting of the gain, as this was done by hand, and to inaccuracies in the manufactured fractal elements, as well as tolerances of other circuit components, such as capacitors C_1 and C_2.

6.2 Numerical analysis

In order to be able to perform a numerical analysis, the circuit has to be converted into a system of differential equations. To get the most accurate results, the complete circuit including all of the discrete sections of the CPE network will be accounted for. Figure 6.8 shows a generalized circuit that can accommodate the CPE on both sides.

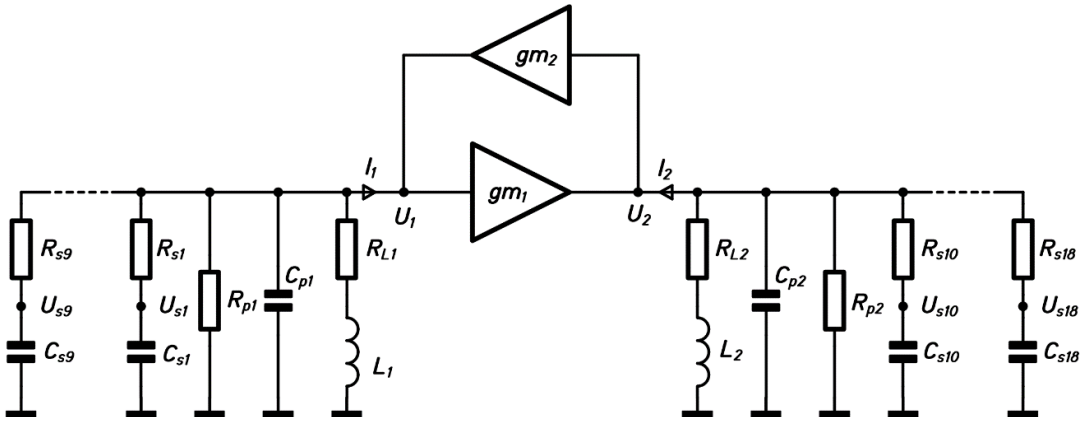

Figure 6.8 Generalized schematic diagram of the approximated fractal order.

We start by defining the relations between circuit variables. Current flowing through a capacitor is defined as

$$i(t) = \frac{dQ}{dt}. \tag{6.1}$$

In our case, voltage is of more interest to us than charge. Substituting the definition of electric charge into the first equation we can get a formula

$$i(t) = \frac{d(C \cdot u)}{dt} = C \cdot \frac{du}{dt}. \tag{6.2}$$

Voltage across an inductor is defined as

$$u(t) = L \cdot \frac{di}{dt}, \tag{6.3}$$

and the voltage across a resistor is simply

$$u(t) = R \cdot i(t). \tag{6.4}$$

Using Kirchhoff laws, the circuit on Figure 6.8 can be analyzed, respecting the directions of all currents in the circuit. Starting with the network containing L_1:

$$u_{L1} = u_1 - u_{R1} \tag{6.5}$$

$$\frac{di_{L1}}{dt} \cdot L_1 = u_1 - R_{L1} \cdot i_{L1}. \tag{6.6}$$

This is then repeated for all time-dependent variables in the system, yielding the following system of differential equations:

$$
\begin{aligned}
&C_{p1} \cdot \frac{du_1}{dt} = -i_{L1} - gm_2(u_2) - \frac{u_1}{R_{p1}} - \sum_{\mathrm{i}=1}^{9} \frac{u_1 - u_{si}}{R_{si}}, \\
&L_1 \cdot \frac{di_1}{dt} = u_1 - R_{L1} \cdot i_1, \\
&C_{s1} \cdot \frac{du_{s1}}{dt} = \frac{u_1 - u_{s1}}{R_1}, \\
&\qquad\qquad \vdots \\
&C_{s9} \cdot \frac{du_{s9}}{dt} = \frac{u_1 - u_{s9}}{R_9}, \\
&C_{p2} \cdot \frac{du_2}{dt} = -i_{L2} - gm_1(u_1) - \frac{u_2}{R_{p2}} - \sum_{\mathrm{i}=10}^{18} \frac{u_2 - u_{si}}{R_{si}}, \\
&L_2 \cdot \frac{di_2}{dt} = u_2 - R_{L2} \cdot i_2, \\
&C_{s10} \cdot \frac{du_{s10}}{dt} = \frac{u_2 - u_{s10}}{R_{10}}, \\
&\qquad\qquad \vdots \\
&C_{s18} \cdot \frac{du_{s18}}{dt} = \frac{u_2 - u_{s18}}{R_{18}}.
\end{aligned}
\tag{6.7}
$$

In order to get a more accurate system model, the non-linear transconductances were modeled including the non-linearities of the system caused by limitation by supply rail voltages, which can be seen on on Figure 5.4 Figure 5.5. This yields wo non-linear transfer functions

$$
gm_1(u_1) = \begin{cases} 6 \cdot 10^{-3}, & \text{for} \quad {u_1}^3 - u_1 > 97, \\ ({u_1}^3 - u_1) \cdot \dfrac{1}{c_1}, & \text{for} \quad 97 \geq {u_1}^3 - u_1 \geq -97, \\ 6 \cdot 10^{-3}, & \text{for} \quad {u_1}^3 - u_1 < -97, \end{cases}
$$

$$gm_2(u_2) = \begin{cases} 30 \cdot 10^{-3}, & \text{for} \quad {u_2}^3 - u_2 > 24, \\ ({u_2}^3 - u_2) \cdot \dfrac{1}{c_1}, & \text{for} \quad 24 \geq 0.1 \cdot {u_2}^3 - u_1 \geq -24, \\ 30 \cdot 10^{-3}, & \text{for} \quad {u_2}^3 - u_2 < -24. \end{cases}$$

The values of c_1 and c_2 will be set equal with those in circuit simulations, as follows:

c_1	c_2	**Configuration**
1100	1100	Integer order system
270	270	C_1 fractal with α = ¼
310	310	C_1 fractal with α = ½
340	340	C_1 fractal with α = ¾
240	240	C_2 fractal with α = ¼
290	290	C_2 fractal with α = ½
340	340	C_2 fractal with α = ¾

Table 6.1 Values of gain for transconductances gm_1 and gm_2

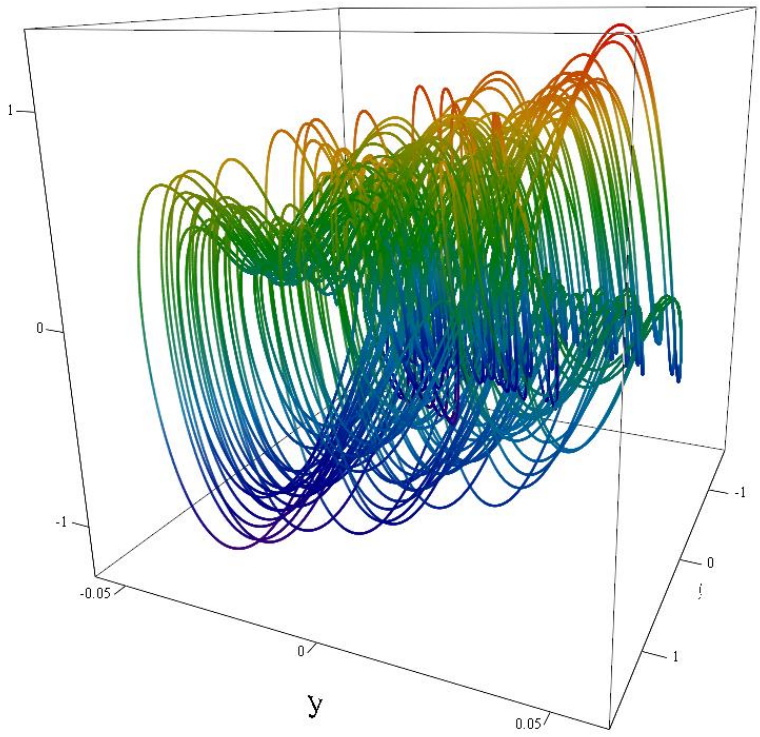

Figure 6.9 Chaotic attractor obtained from numerical analysis of the integer order system.

Numerical analysis was performed using MathCad software, utilizing a fixed step solver. The integer order system generated interesting attractors, comparable to the ones obtained from the SPICE simulations and real measurements. The results with fractal element approximations were less accurate. While chaotic behavior can be observed, it only lasts for a while, before stabilizing on a fixed point located at 0. The chaotic attractor from the integer order system is depicted on Figure 6.9. while other results are available in the appendix section.

Discrepancies in the numerical data can be attributed to many factors. While significant effort was made to ensure accurate representation of the real circuit, there are numerous factors still not accounted for. The modified transfer functions are more representative of the simulated circuit, they are still not entirely representative of reality. Other non-idealities in the circuit are present which the circuit model accounts for, but the numerical model does not. The rather simple type of solver used will also have effect on the results. PSpice uses a more advanced numerical integration method. This combined with more accurate circuit model will yield results closer to reality.

CONCLUSION

In this thesis, a study of fractional order chaotic system was performed. Multiple constant phase elements were designed, simulated, manufactured, and verified by measurements. Next, a chaotic system was synthesized from a set of differential equations, which as well was simulated, manufactured, and verified by measurements. This system was then converted into a fractional order system by substituting capacitors in the circuit by fractional order approximations. The chaotic order fractional system was then verified both by measurements and by numerical analysis.

The method used to synthesize fractal elements proved very capable and the process of creating them was very straightforward. The manufactured fractal elements were accurate enough to be used in the fractional order chaotic system. It was however discovered that measurement of fractal elements with the impedance norm set high is difficult. Parasitic properties of the measuring setup and the device itself have negative influence on the results. If not application critical, it is desirable to use fractal elements with low impedance norm.

The synthesis of the chaotic system was also successful, yielding a working circuit. However, a large number of active elements were used in the realized circuit. The AD633 is a rather exotic component and very costly. Another solution of the synthesis was later discovered that contained only 4 analog multipliers, which would have been preferred. The dynamic range of the non-linear transconductances was sufficient for chaos to manifest in the circuit, however multiple of the measured attractors show, that the circuit would benefit from a greater dynamic range. This could be achieved by further optimizing the synthesized circuit. There are noticeable discrepancies between the obtained data from all realizations of the dynamic system, the circuit simulation, the measurement and the numerical analysis. While this is inevitable when working with chaotic systems, which are inherently sensitive to even the most subtle changes in parameters, a greater correlation between the data could have been achieved given more time spend optimizing and more accurate models.

LITERATURE

[1] ORTIGUEIRA, Manuel. *An introduction to the fractional continuous-time linear systems*: the 21st century systems. Online. IEEE Circuits and Systems

[2] Magazine. 2008, roč. 8, č. 3, s. 19-26. ISSN 1531-636X. Dostupné z: https://doi.org/10.1109/MCAS.2008.928419. [cit. 2023-12-29].

[3] PETRZELA, J. *Accurate Constant Phase Elements Dedicated for Audio Signal Processing*. Online. Applied Sciences. 2019, roč. 9, č. 22. ISSN 2076-3417. Dostupné z: https://doi.org/10.3390/app9224888. [cit. 2023-12-29].

[4] SIVARAMA KRISHNA, M.; DAS, S.; BISWAS, K. a GOSWAMI, B.. *Fabrication of a Fractional Order Capacitor With Desired Specifications: A Study on Process Identification and Characterization*. Online. IEEE Transactions on Electron Devices. 2011, roč. 58, č. 11, s. 4067-4073. ISSN 0018-9383. Dostupné z: https://doi.org/10.1109/TED.2011.2166763. [cit. 2023-12-29].

[5] ČAJKA, Josef a KVASIL, Josef. Teorie lineárních obvodů: (analýza lineárních a linearizovaných elektrických obvodů). Teoretická knižnice inženýra. Praha: SNTL, 1979.

[6] BRUTON, L. *Network Transfer Functions Using the Concept of Frequency-Dependent Negative Resistance*. Online. IEEE Transactions on Circuit Theory. 1969, roč. 16, č. 3, s. 406-408. ISSN 0018-9324. Dostupné z: https://doi.org/10.1109/TCT.1969.1082989. [cit. 2023-12-29].

[7] RADWAN, A. G. a SALAMA, K. N. *Fractional-Order RC and RL Circuits. Online. Circuits, Systems, and Signal Processing*. 2012, roč. 31, č. 6, s. 1901-1915. ISSN 0278-081X. Dostupné z: https://doi.org/10.1007/s00034-012-9432-z. [cit. 2023-12-29].

[8] BISWAS, K.; BOHANNAN, G.; CAPONETTO, R.; MENDES LOPES, A. a TENREIRO MACHADO, J. A. *Fractional-order devices*. Cham, Switzerland: Springer, 2017. ISBN 978-3-319-54459-5.

[9] CARLSON, G. a HALIJAK, C. *Approximation of Fractional Capacitors (1/s)^(1/n) by a Regular Newton Process*. Online. IEEE Transactions on Circuit Theory. 1964, roč. 11, č. 2, s. 210-213. ISSN 0018-9324. Dostupné z: https://doi.org/10.1109/TCT.1964.1082270. [cit. 2023-12-29].

[10] SOTNER, R.; POLAK, L.; JERABEK, J. a PETRZELA, J. Simple two operational transconductance amplifiers-based electronically controllable bilinear two port for fractional-order synthesis. Online. Electronics Letters. 2018, roč. 54, č. 20, s. 1164-1166. ISSN 0013-5194. Dostupné z: https://doi.org/10.1049/el.2018.5575. [cit. 2023-12-29].

[11] PETRZELA, Jiri; SOTNER, Roman a GUZAN, Milan. *Implementation of constant phase elements using low-Q band-pass and band-reject filtering sections*. Online. In: 2016 International Conference on Applied Electronics (AE). IEEE, 2016, s. 205-210. ISBN 978-80-261-0602-9. Dostupné z: https://doi.org/10.1109/AE.2016.7577274. [cit. 2023-12-29].

[12] VALSA, J.; DVOŘÁK, P. and FRIEDL M. *Network Model of the CPE*. Online. Radioengineering. 2011, roč. 20, č. 3, s. 619-626. ISSN 1210-2512. Dostupné z: https://www.radioeng.cz/fulltexts/2011/11_03_619_626.pdf. [cit. 2023-12-29].

[13] BRAUN, Jaromír. *Analýza lineárních obvodů a soustav*. Teoretická knižnice inženýra. Praha: Státní nakladatelství technické literatury, 1973.

[14] VALSA, Juraj a VLACH, Jiri. *RC models of a constant phase element*. Online. International Journal of Circuit Theory and Applications. 2013, roč. 41, č. 1, s. 59-67. ISSN 0098-9886. Dostupné z: https://doi.org/10.1002/cta.785. [cit. 2023-12-29].

[15] Analog Devices. *AD844*. Online katalógový list. posledné úpravy 2017. Dostupné z: https://www.analog.com/media/en/technical-documentation/data-sheets/ad844.pdf. [cit. 2023-12-29].

[16] KASHYAP, Katyayani; SARMA, Manash Pratim a SARMA, Kandarpa Kumar. *Chaotic spread spectrum modulation — A hardware implementation approach*. Online. In: 2014 International Conference on Advances in Electronics Computers and Communications. IEEE, 2014, s. 1-6. ISBN 978-1-4799-5496-4. Dostupné z: https://doi.org/10.1109/ICAECC.2014.7002432. [cit. 2023-12-29].

[17] LI, Guodong; XU, Xiangliang a ZHONG, Huiyan. *A image encryption algorithm based on coexisting multi-attractors in a spherical chaotic system*. Online. Multimedia Tools and Applications. 2022, roč. 81, č. 22, s. 32005-32031. ISSN 1380-7501. Dostupné z: https://doi.org/10.1007/s11042-022-12853-9. [cit. 2023-12-29].

[18] MATSUMOTO, T. *A chaotic attractor from Chua's circuit*. Online. IEEE Transactions on Circuits and Systems. 1984, roč. 31, č. 12, s. 1055-1058. ISSN 0098-4094. Dostupné z: https://doi.org/10.1109/TCS.1984.1085459. [cit. 2023-12-29].

[19] WANG, Ning; LI, Chengqing; BAO, Han; CHEN, Mo a BAO, Bocheng. *Generating Multi-Scroll Chua's Attractors via Simplified Piecewise-Linear Chua's Diode*. Online. IEEE Transactions on Circuits and Systems I: Regular Papers. 2019, roč. 66, č. 12, s. 4767-4779. ISSN 1549-8328. Dostupné z: https://doi.org/10.1109/TCSI.2019.2933365. [cit. 2023-12-29].

[20] PETRZELA, Jiri. *Chaos in Analog Electronic Circuits: Comprehensive Review, Solved Problems, Open Topics and Small Example*. Online. Mathematics. 2022, roč. 10, č. 21. ISSN 2227-7390. Dostupné z: https://doi.org/10.3390/math10214108. [cit. 2023-12-29].

[21] HRAMOV, Alexander E. a KORONOVSKII, Alexey A. *An approach to chaotic synchronization*. Online. Chaos: An Interdisciplinary Journal of Nonlinear Science. 2004, roč. 14, č. 3, s. 603-610. ISSN 1054-1500. Dostupné z: https://doi.org/10.1063/1.1775991. [cit. 2023-12-29].

[22] PETRZELA, J. *Chaotic behaviour of state variable filters with saturation-type integrators*. Online. Electronics Letters. 2015, roč. 51, č. 15, s. 1159-1161. ISSN 0013-5194. Dostupné z: https://doi.org/10.1049/el.2015.1563. [cit. 2023-12-29].

[23] KVASIL, Josef a ČAJKA, Josef. *Úvod do syntézy lineárních obvodů*. Praha: SNTL, 1981.

[24] JUN-JIE, Lu a CHONG-XIN, Liu. *Realization of fractional-order Liu chaotic system by circuit*. Online. Chinese Physics. 2007, roč. 16, č. 6, s. 1586-1590. ISSN 1009-1963. Dostupné z: https://doi.org/10.1088/1009-1963/16/6/016. [cit. 2023-12-29].

[25] TRIPATHY, Madhab Chandra; BISWAS, Karabi a SEN, Siddhartha. *A Design Example of a Fractional-Order Kerwin–Huelsman–Newcomb Biquad Filter with Two Fractional Capacitors of Different Order*. Online. Circuits, Systems, and Signal Processing. 2013, roč. 32, č. 4, s. 1523-1536. ISSN 0278-081X. Dostupné z: https://doi.org/10.1007/s00034-012-9539-2. [cit. 2023-12-29].

[26] ITOH, MAKOTO. *Synthesis of electronic circuits for simulating nonlinear dynamics*. Online. International Journal of Bifurcation and Chaos. 2011, roč. 11, č. 03, s. 605-653. ISSN 0218-1274. Dostupné z: https://doi.org/10.1142/S0218127401002341. [cit. 2023-12-29].

[27] SORDI, Alexandre. *Chua's oscillator: an introductory approach to chaos theory*. Online. Revista Brasileira de Ensino de Física. 2021, roč. 43. ISSN 1806-9126. Dostupné z: https://doi.org/10.1590/1806-9126-rbef-2020-0437. [cit. 2023-12-29].

[28] SEDAGHAT, H. *Folding Difference and Differential Systems into Higher Order Equations*. Online. Virginia Commonwealth University. 2013. Dostupné z: https://arxiv.org/pdf/1403.3995.pdf. [cit. 2023-12-29].

[29] Electronic Associates, Inc. *Handbook of Analog Computation*, *Second edition*. Princeton, New Jersey, 1967. Dostupné z: https://archive.org/details/bitsavers_eaiEAIHandtionMay71_23989175. [cit. 2023-12-29].

[30] Analog Devices. *AD633*. Online katalógový list. posledné úpravy 2015. Dostupné z: https://www.analog.com/media/en/technical-documentation/data-sheets/ad633.pdf. [cit. 2023-12-29].

[31] Texas Instruments. *TL07xx Low-Noise FET-Input Operational Amplifiers*. Online katalógový list. posledné úpravy 2023. Dostupné z: https://www.ti.com/lit/ds/symlink/tl072.pdf. [cit. 2023-12-29].

LIST OF SYMBOLS AND ABBREVIATIONS

Abbreviations:

CPE	constant phase element
SMD	surface mount device
THT	through hole technology
PCB	printed circuit board

Symbols:

U	voltage	[V]
I	current	[A]
R	resistance	[Ω]
C	capacitance	[F]
L	inductance	[H]
Z	impedance	[Ω]
Y	admittance	[S]
D	fractance	[F/s$^{1-\alpha}$]
G	conductance	[S]
Q	quality factor	[-]
Ω	frequency norm	[Hz]
ω	angular frequency	[rad/s]
ζ	impedance norm	[Ω]
φ	phase angle	[°]
s	Laplace variable	[rad/s]
f	frequency	[Hz]
T	time	[s]
gm	transconductance	[A/V]
$\|\|$	parallel combination	
$\&$	series combination	

LIST OF APENDECIES

Appendix A - Pictures

A.1 Top view on the chaotic system PCB

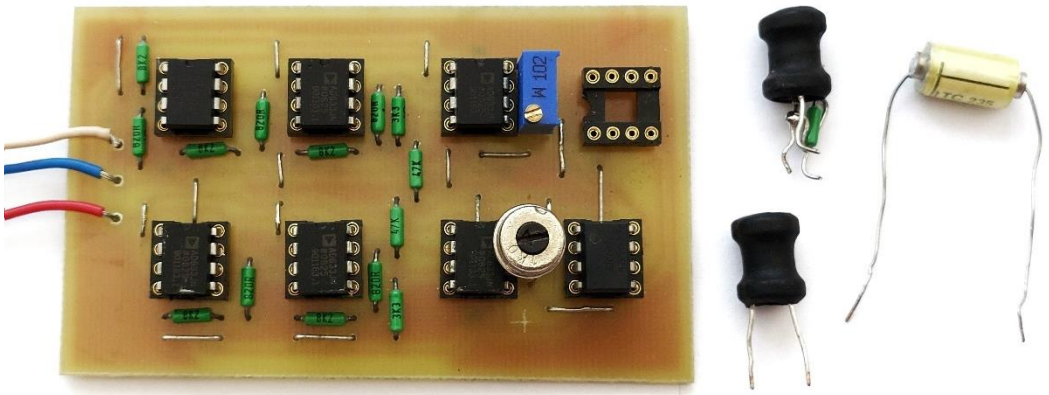

A.2 Bottom view on the chaotic system PCB

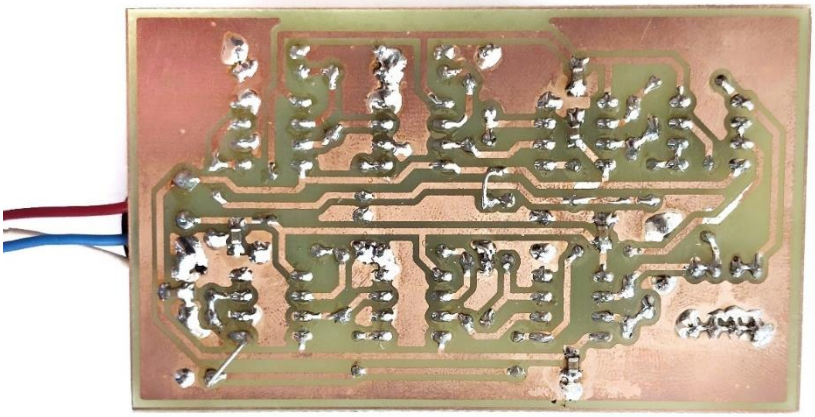

A.3 View of the 3 CPE PCB's

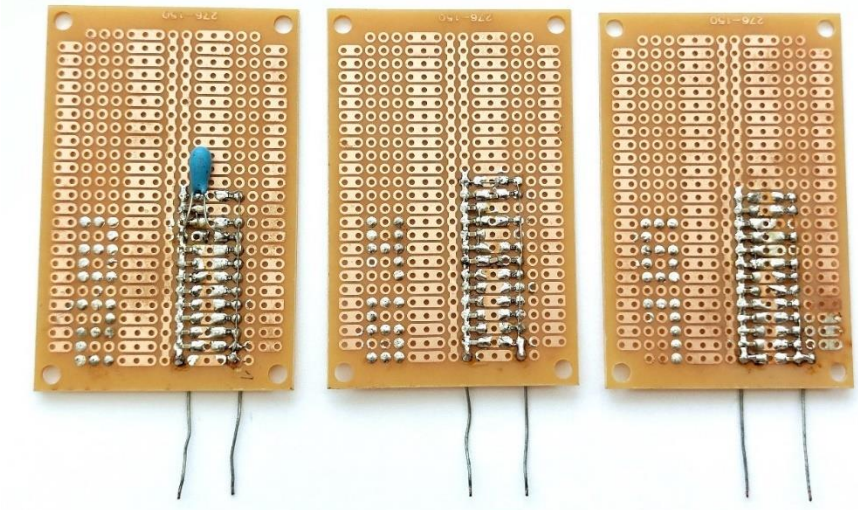

Appendix B - Documentation of the chaotic circuit PCB

B.1 Top assembly

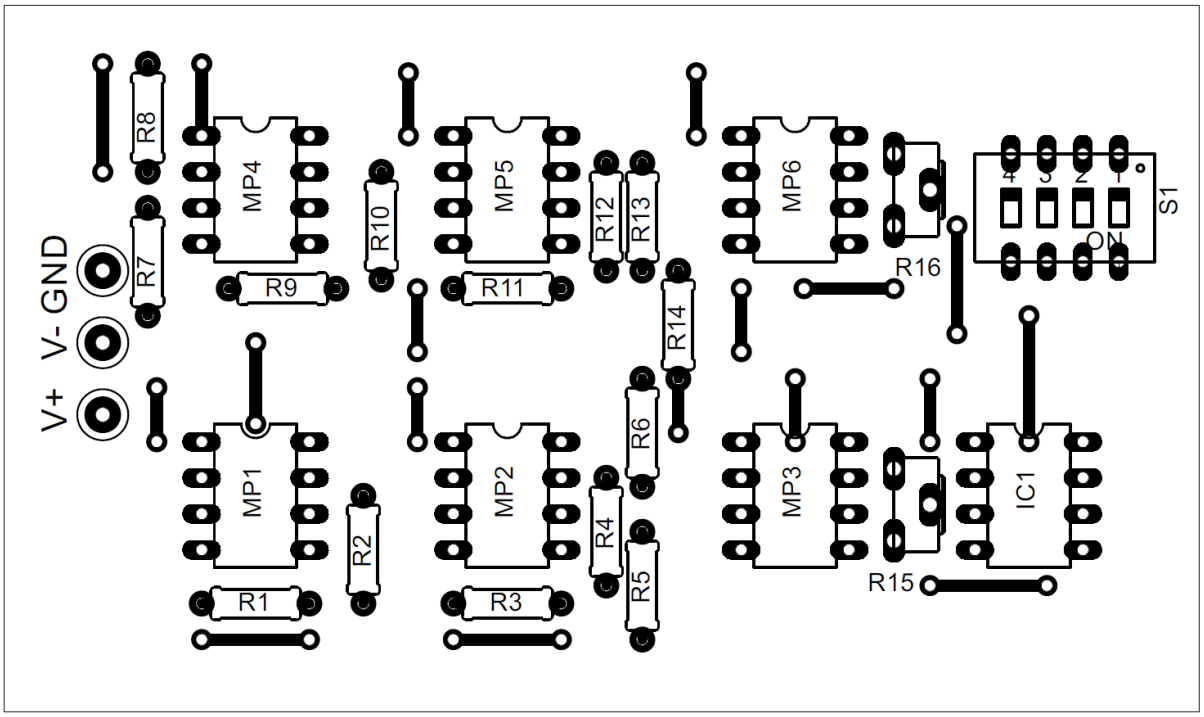

B.2 Bottom assembly

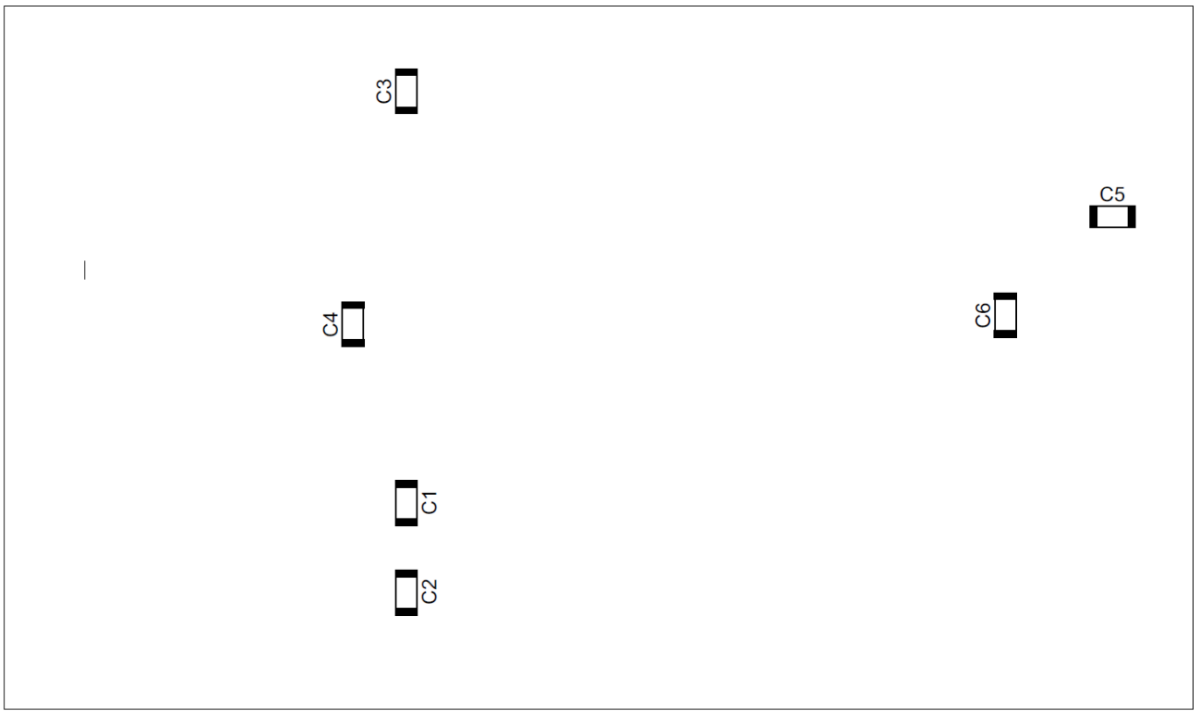

B.3 PCB layout

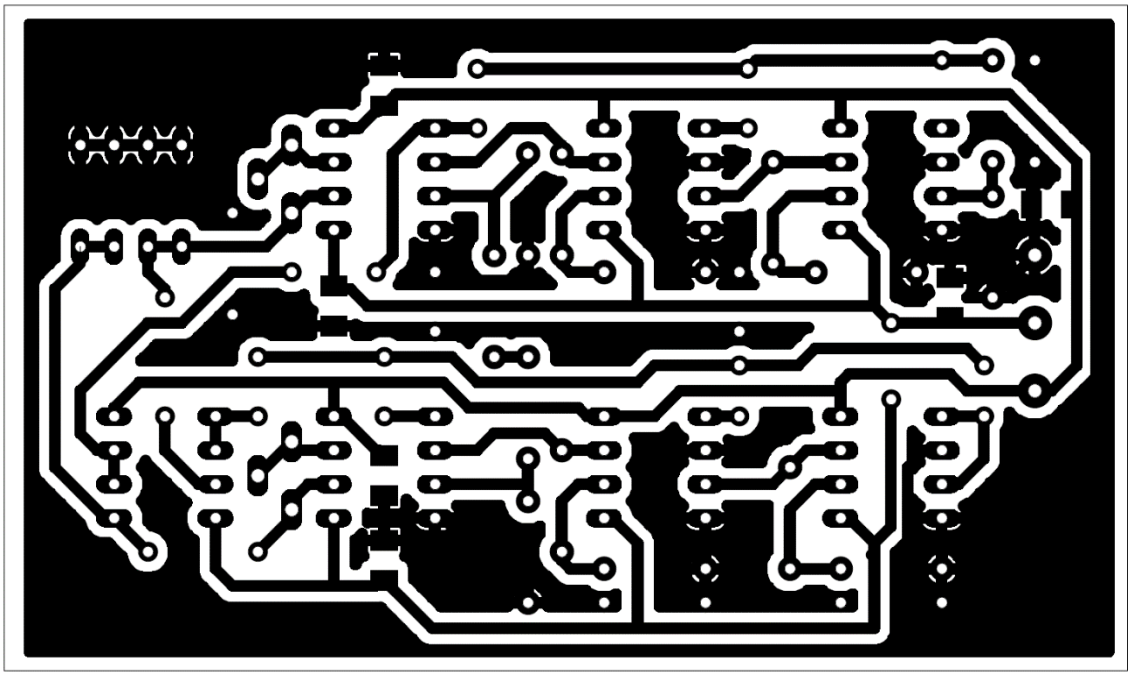

B.4 List of components

Name	Value	Type	Tolerance	Name	Value	Type	Tolerance
R1	8.2 kΩ	TR191	±5%	R16	1 kΩ	TP095	±5%
R2	820 Ω	TR191	±5%	MP1	AD633	DIP-8	-
R3	8.2 kΩ	TR191	±5%	MP2	AD633	DIP-8	-
R4	820 Ω	TR191	±5%	MP3	AD633	DIP-8	-
R5	3.3 kΩ	TR191	±5%	MP4	AD633	DIP-8	-
R6	47 kΩ	TR191	±5%	MP5	AD633	DIP-8	-
R7	820 Ω	TR191	±5%	MP6	AD633	DIP-8	-
R8	8.2 kΩ	TR191	±5%	IC1	TL072	DIP-8	-
R9	8.2 kΩ	TR191	±5%	C1	100 nF	0603	±5%
R10	820 Ω	TR191	±5%	C2	100 nF	0603	±5%
R11	8.2 kΩ	TR191	±5%	C3	100 nF	0603	±5%
R12	820 Ω	TR191	±5%	C4	100 nF	0603	±5%
R13	3.3 kΩ	TR191	±5%	C5	100 nF	0603	±5%
R14	47 kΩ	TR191	±5%	La	33 mH	RL8010	±5%
R15	1 kΩ	TP095	±5%	Lb	33 mH	RL8010	±5%

B.5 Schematic diagram of the chaotic circuit

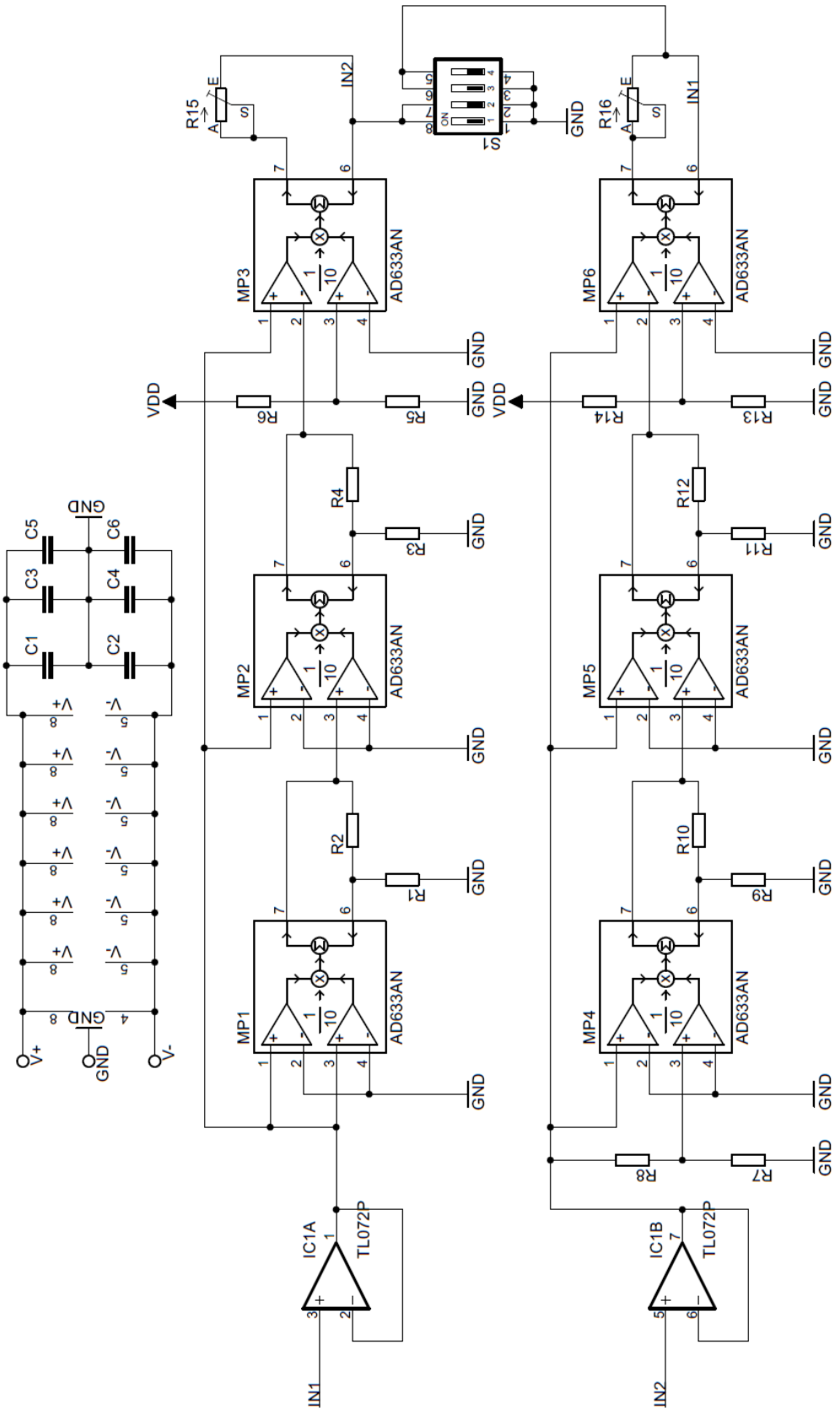

Appendix C - Attractors obtained from numerical analysis. Plotted are the values of U_1, U_2 and I_2.

C.1 Attractor with C_2 fractal and α = ¼

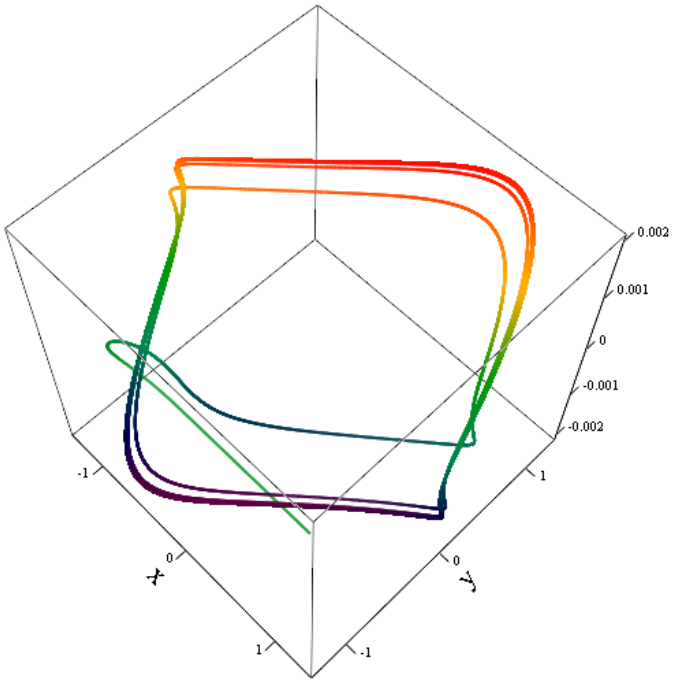

C.2 Attractor with C_2 fractal and α = ½

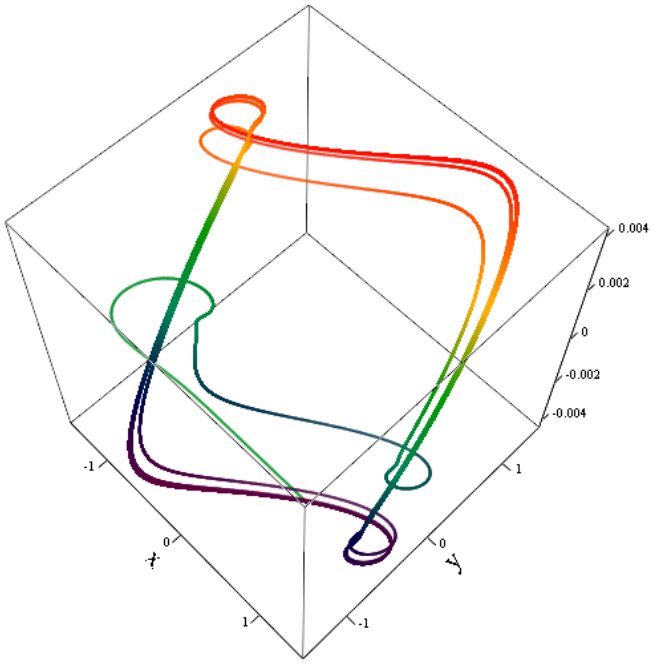

C.3 Attractor with C2 fractal and α = ¾

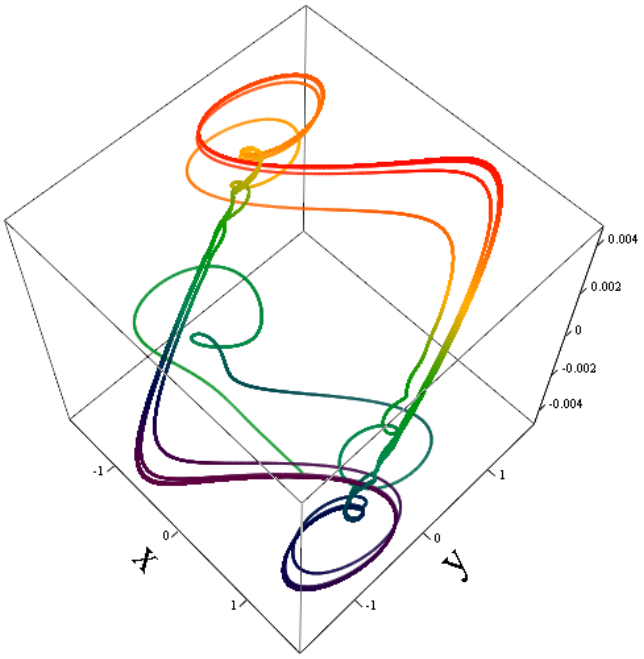

C.4 Attractor with C1 fractal and α = ¼

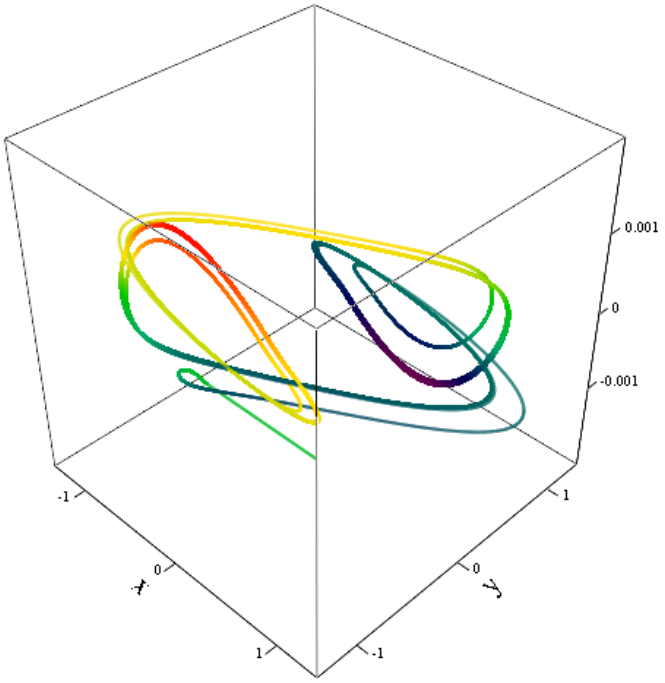

C.5 Attractor with C1 fractal and α = ½

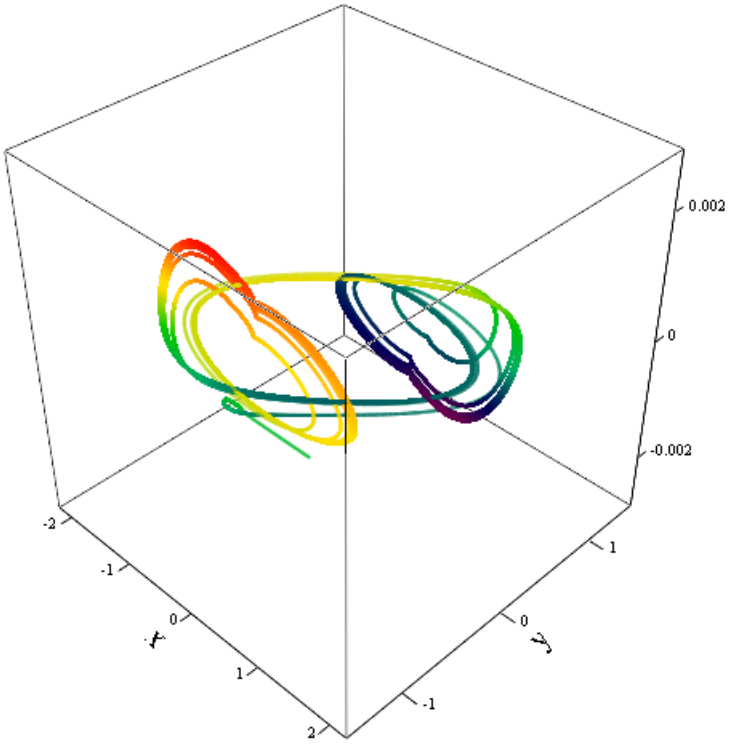

C.6 Attractor with C1 fractal and α = ¾